

---

# Precise GPS Position and Attitude

---

*GPS Technology - 2007*

---

Group - 07gr1048

*Volodymyr Petrovskyy  
Vyacheslav Tretyak*

---

Spring 2007  
AALBORG UNIVERSITY



# Faculty of Engineering and Science

Aalborg University



## Institute of electronic systems

**THEME:**

GNSS Signals and Receiver Technology

**SUBJECT:**

Global Positioning System

**TITLE:**

Precise GPS Position and Attitude

**PROJECT PERIOD:**

1 February 2007 - 7 June 2007

**GROUP:** 07gr1048**GROUP MEMBERS:**

Volodymyr Petrovskyy  
Vyacheslav Tretyak

**SUPERVISOR:**

Kai Borre

**NUMBER OF COPIES:** 4**NUMBER OF PAGES**

**IN REPORT:** 66

**NUMBER OF PAGES**

**IN APPENDIX:** 6

**TOTAL NUMBER OF PAGES:** 72**Abstract**

The need of accuracy in GPS positioning is constantly growing. Carrier phase observations are ambiguous, and much more precise compared to code phase observations. This project presents a software, which provides precise positioning and attitude determination in post processing mode of a moving tractor in a field. The results showed the position and attitude accuracy of one centimeter and  $0.5^\circ$ , respectively. Furthermore, to present the nature of observations, code phase and carrier phase observations are implemented in a software receiver. However, the carrier frequency accuracy of the PLL output in the tracking channels produced lower position accuracy compared to the position accuracy obtained from code phase observations in this software receiver.

# Preface

---



This document reports the work of group 07gr1048 in the 10<sup>th</sup> semester. It includes five chapters. The first gives an introduction to GPS system. Problem statement is described in the second chapter followed by implementation in the third chapter. Results and discussion are presented in the ongoing forth chapter. Conclusions are given in the last fifth chapter. Attached to the report DVD contains all programs and functions developed in the project. The reader is welcome to use it: the user-friendly GUIs are described in the appendix.

References are given as abbreviations of literature titles in square brackets that correspond to entries in the bibliography section at the end of the document. A list of figures and a list of tables are also provided.

We want to thank our supervisor professor Kai Borre for guiding us through the course of the project, as well as research engineer Darius Plausinaitis, research assistants Kostas Dragunas and Vitalijus Linikas for providing valuable information and advice on difficulties, which arose at various stages of our work. It is also appropriate here to say a word of thanks to Lars Holten Hansen, who allowed us to use his tractor to make observations in his farm fields.

Aalborg, June 4, 2007

Volodymyr Petrovskyy .....  
(signature)

Vyacheslav Tretyak .....  
(signature)

# Contents

<b>1</b>	<b>Introduction</b>	<b>5</b>
1.1	GPS Measurement Biases and Errors . . . . .	5
1.1.1	Ephemeris Errors . . . . .	5
1.1.2	Satellite Clock Errors . . . . .	6
1.1.3	Ionospheric Effects . . . . .	6
1.1.4	Tropospheric Effects . . . . .	6
1.1.5	Multipath . . . . .	6
1.1.6	Overall Error Budget . . . . .	7
1.2	GPS Signal Components, Structure, and Characteristics . . . . .	7
1.2.1	Two L-band Carrier Waves . . . . .	7
1.2.2	Ranging Codes . . . . .	7
1.2.3	Navigation Message . . . . .	8
<b>2</b>	<b>Problem Formulation</b>	<b>9</b>
2.1	Problem Description . . . . .	9
2.2	Problem Statement . . . . .	9
2.3	Results . . . . .	10
<b>3</b>	<b>Implementation</b>	<b>11</b>
3.1	Coordinate Systems . . . . .	11
3.2	Satellite Orbits . . . . .	12
3.2.1	Keplerian Elements . . . . .	13
3.2.2	Keplerian Motion in Orbital and ECEF Coordinate Systems . . . . .	13
3.2.3	Satellite Position and Velocity . . . . .	16
3.3	Doppler Effect . . . . .	19
3.4	Observations in Software Receiver . . . . .	20
3.4.1	Acquisition . . . . .	20
3.4.1.1	C/A-code Generation . . . . .	20
3.4.1.2	Estimation of Signal Frequency and Code Phase Shift . . . . .	22
3.4.1.3	Fine Carrier Frequency Resolution . . . . .	22
3.4.2	Tracking and Data Decoding . . . . .	26
3.4.3	Code Phase Observations . . . . .	28
3.4.4	Carrier Phase Observations . . . . .	28
3.5	Point Positioning . . . . .	35
3.6	Differential Positioning . . . . .	37
3.6.1	Single Difference of Code Observables . . . . .	37
3.6.2	Double Difference of Code Observables . . . . .	38

## CONTENTS

---

3.6.3	Double Difference of Phase Observables . . . . .	40
3.6.4	Ambiguity Resolution . . . . .	40
3.6.5	Cycle Slip Detection and Repair . . . . .	43
3.7	Computing Positions by Kalman Filter . . . . .	44
3.8	Attitude Determination . . . . .	46
3.8.1	Background . . . . .	46
3.8.2	Coordinate Frame Definition . . . . .	47
3.8.3	System Setup . . . . .	48
3.8.4	Roll, Pitch, and Yaw Determination . . . . .	48
<b>4</b>	<b>Results and Discussion</b>	<b>53</b>
<b>5</b>	<b>Conclusions</b>	<b>65</b>
5.1	Future Considerations and Improvements . . . . .	65
<b>A</b>	<b>Data contained in the DVD</b>	<b>67</b>
<b>B</b>	<b>Working Process</b>	<b>68</b>

# Chapter 1

## Introduction

The Global Positioning System (GPS) is a satellite-based navigation system for accurate and instantaneous position determination and timing. GPS has many applications which include control, timing and synchronization of telecommunications and power networks, deformation monitoring and analysis, polar and tectonic plate motion determination, etc. The working principles of GPS are based on the principle of trilateration: the position of unknown point is determined by measuring ranges to four or more known points. In this particular case, the known points are the position of the satellites moving in nearly circular orbits in space and the unknown point is the position of the receiver. Each satellite transmits a unique radio signal code which is received passively by the receiver, and the time is measured that it takes the signal to travel from the satellite to the receiver. The distance is basically the product of the transit time and the velocity of the radio signal. Nevertheless, there are various sources of error which affect the accuracy of the position determination in GPS. The impact of these errors can be canceled or significantly reduced by the method of Differential GPS (DGPS).

### 1.1 GPS Measurement Biases and Errors

GPS measurements are affected by biases and errors. Their combined magnitude will affect the accuracy of the position determination. There are several sources of bias with varying characteristics of magnitude, periodicity, satellite-receiver dependency, etc. Among these biases are ephemeris errors, satellite clock errors, receiver clock errors, ionospheric effects, and tropospheric effects.

#### 1.1.1 Ephemeris Errors

The ephemeris information used to calculate the satellite position is based on the observations from the monitor stations of the space segment. The data is processed at the Master Control Station and the satellite navigation message information is uploaded to every satellite. The ephemeris error is, therefore, the discrepancy between the true position of the satellite and its broadcast ephemeris. This grows from the time of upload by a monitor station until the next upload. Parkinson & Spilker Jr. (1996) estimate the root-mean-square (rms) error as 2.1 m. In recent years it might be as low as one meter.

## CHAPTER 1. INTRODUCTION

---

### 1.1.2 Satellite Clock Errors

Although GPS satellites use high quality cesium or rubidium atomic clocks for time-keeping and signal synchronization, there are unavoidable clock errors which change with time. Rubidium oscillator is correct within  $10^{-11}$ -  $10^{-12}$  s and that of cesium is correct within  $10^{-12}$ - $10^{-13}$  s. The offset could reach  $10^{-7}$  seconds in a day; multiplied by the velocity of light the error can reach 30 m.

### 1.1.3 Ionospheric Effects

The ionosphere extends between approximately 50 and 1000 km above the earth. It is characterized by the presence of free electrons and positively charged ions. This is a result of the gas molecules being excited by solar radiation. Since the number of electrons equals the number of ions the layer is natural but the effect of the ionosphere on the signal propagation can be attributed to the electrons because they have a much larger mobility due to their smaller mass. The Total Electron Content (TEC) equals the number of free electrons in the column of a unit area along which the signal travels between the satellite and the receiver. TEC varies as a function of latitude of the receiver, the season, the time of the day the observation of the satellite signal is being made and the level of solar activity at the time of observation. As the electromagnetic GPS signal propagates through the medium, dispersion occurs and the free electrons delay the pseudorange and advance the carrier phase by equal magnitude. The amount is directly proportional to the TEC and inversely proportional to the carrier frequency. GPS frequency delays or advances can be up to 36 m for signals at the zenith to as much as 100 m for observations made at the receiver's horizon [Eng01].

### 1.1.4 Tropospheric Effects

The troposphere extends from the surface of the earth to about 50 km above the earth and it is neither ionized nor dispersive. GPS signals traveling through this medium will experience delay that is a function of elevation and altitude of the receiver. Tropospheric effect depends on the atmospheric pressure, temperature and humidity. The bias ranges from approximately 2.5m for satellites at the zenith to about 25m depending upon the satellite elevation angle [Eng01].

### 1.1.5 Multipath

Multipath effects are propagation errors arising from interference of the direct signal by reflected signals from water, metallic surfaces and nearby buildings. The combined direct and reflected signals will give rise to incorrect observations. The remedies for multipath lie in site selection and effective antenna design to filter out multipath effects using advanced signal processing.

## 1.2. GPS SIGNAL COMPONENTS, STRUCTURE, AND CHARACTERISTICS

---

### 1.1.6 Overall Error Budget

Standard errors of a single frequency receiver as given in [Bor97] expressed in position uncertainty in meters presented in Table 1.1 . As it can be seen the most significant errors come from ionosphere and then multipath, satellite clock, and others. Most of these errors can be corrected in DGPS except multipath which is site dependent.

Table 1.1: Overall error budget

Source	Impact, m
Ephemeris data	2
Satellite clock	2
Ionosphere	4
Troposphere	0.5 - 1
Multipath	0 - 2

## 1.2 GPS Signal Components, Structure, and Characteristics

Each satellite transmits a unique navigational signal centered on two L-band frequencies of the electromagnetic spectrum. All satellite transmissions are coherently derived from the fundamental frequency of 10.23 MHz generated by the atomic clock onboard. The satellite signal consists of the following components: the two L-band carrier waves, the ranging codes and the navigation message. These are discussed below.

### 1.2.1 Two L-band Carrier Waves

The two L-band carrier waves are L1 at 1575.42 MHz and L2 at 1227.60 MHz. They are generated by multiplying the fundamental frequency (10.23 MHz) by 154 and 120, respectively. These carrier waves provide the means by which the ranging codes and the navigation message are transmitted to the receiver.

### 1.2.2 Ranging Codes

GPS codes are binary strings of zeros and ones. The two basic codes are the Precise Code (P-Code) and the Coarse Acquisition Code (C/A Code). The P-Code generated at the fundamental frequency (i.e. 10.23 MHz) is available on both both L1 and L2. Each satellite repeats its portion of the P-Code every seven days, and the entire code is renewed every 37 weeks. The precision P-Code is the principal code used for military navigation. The C/A Code is generated at 1.023 MHz (i.e. one-tenth of the fundamental frequency). Each satellite broadcasts a completely unique C/A Code modulated on only the L1 frequency and it is repeated every millisecond.

Table 1.2: Components of satellite signal

Composition	Frequency, MHz	
Fundamental frequency	$f_0$	= 10.23
Carrier L1	$154 f_0$	= 1575.42 ( $\simeq 19.0$ cm)
Carrier L2	$120 f_0$	= 1227.60 ( $\simeq 24.4$ cm)
P-code	$f_0$	= 10.23
C/A-code	$f_0/10$	= 1.023
W-code	$f_0/20$	= 0.5115
Navigation message	$f_0/204600$	$= 50 \cdot 10^{-6}$

### 1.2.3 Navigation Message

The navigation message is generated at a low frequency of 50 Hz and is modulated on both L1 and L2 carrier frequencies. It contains information on the ephemerides of the satellites, GPS time, clock behavior, and system status messages. Table 1.2 taken from [B. 01] lists all composite parts of GPS signals.

The signal is modeled as

$$s(t) = \sqrt{2P_C}x(t)D(t)\sin(2\pi f_{L1}t + \Theta_{L1}) + \sqrt{2P_{Y,L1}}y(t)D(t)\cos(2\pi f_{L1}t + \Theta_{L1}) + \sqrt{2P_{Y,L2}}y(t)D(t)\cos(2\pi f_{L2}t + \Theta_{L2})$$

where  $P_C$ ,  $P_{Y,L1}$ ,  $P_{Y,L2}$  are the signal powers carrying C/A-code on L1, and P(Y)-code on L1 and L2. Chips  $x$  and  $y$  are C/A- and P(Y)-code sequences; D denotes the navigation data bit stream;  $f_{L1}$  and  $f_{L2}$  are the carrier frequencies corresponding to L1 and L2, respectively; and  $\Theta_{L1}$  and  $\Theta_{L2}$  are phase offsets.

The modulation of a carrier by a binary code spreads the signal energy, initially concentrated at a single frequency, over a wide frequency band: over 2 MHz for the C/A-code and about 20 MHz for the P(Y)-code, centered at the carrier frequency. While the signal power is unchanged, this step reduces the power spectral density below that for the background RF radiation. Such signals, referred to as spread spectrum signals, have many properties which make them attractive for use in communication and navigation. The signal energy can be "de-spread" in a receiver, if the code is known. In principle, keeping a code secret limits access to the signal.

C/A-code, also known as pseudo-random noise (PRN) sequences or Gold codes, are nearly orthogonal to each other. The PRN sequences are nearly uncorrelated for all shifts. Another property of PRN sequence is that it is uncorrelated with itself except for the zero shift.

# **Chapter**

# **2**

## **Problem Formulation**

This chapter contains problem statement of the project, scope, limitations, technical specifications and development stages.

### **2.1 Problem Description**

Applications of GPS are constantly being developed. There are many areas which require up to cm-level accuracy of positions, for instance, precision farming, surveying and mapping, aviation, etc. In aviation attitude determination is used for the orientation of an aircraft with respect to the horizon. The pitch angle specifies the orientation of the aircraft's longitudinal axis. The roll angle specifies whether the aircraft is banked left or right, or whether its wings are parallel to the horizon. Main advantages of using GPS in agriculture are reduced fuel costs, decreased driver fatigue, eliminated overlap. The level of required accuracy differs depending on the performed agricultural operation. For spreading and spraying the accuracy of  $\pm 10$  cm is sufficient for most farmers. For agricultural operations like seeding, harvesting, cultivating, and plowing the accuracy of  $\pm 10$  cm is definitely too low while  $\pm 2$  cm would be sufficient.

We focus on developing software capable of providing positions with cm-level accuracy. Many errors of GPS measurements can be eliminated in double difference of observations. Carrier phaser observations are ambiguous, and much more precise compared to code phase observations. Positioning based on carrier phase observations can reach accuracy better than one centimeter.

Furthermore, using differential positioning makes it possible to obtain accurate attitude determination of a vehicle such as roll, pitch, and yaw, although the positions are not so accurate.

### **2.2 Problem Statement**

Autonomous guidance of agricultural vehicles is not a new idea. Previous attempts to control agricultural vehicles have been largely unsuccessful due to sensor limitations. Some control systems require cumbersome auxiliary guidance mechanisms in or around the field, while others rely on a camera system requiring clear daytime weather and field markers that can be deciphered by visual pattern recognition. GPS-based systems are already being used in a number of land vehicle applications including agriculture. The accuracy of  $\pm 30\text{-}50$  cm can be achieved by applying OmniSTAR-HP differential corrections or augmenting GPS system with WAAS or EGNOS. However, the accuracy of cm-level in vehicle position determination and  $0.5^\circ$  accuracy in attitude determination can be achieved using precise differential carrier phase measurements

## CHAPTER 2. PROBLEM FORMULATION

---

of satellite signals.

The main goal of the project is to design software for different positioning setups based on carrier phase observations. The expected accuracy of positioning and attitude determination should be in the range of one centimeter and  $0.5^\circ$ , respectively.

The scope of the project is limited to investigation of different positioning setup accuracies for one set of measurements. To understand the nature of carrier phase observations, an existing software receiver is modified to produce carrier phase observations.

In order to achieve the defined objectives the project is divided as follows:

- Implementation of carrier phase observations based on PLL output of a tracking channel in existing software receiver.
- Three geodetic hardware receivers are put on a tractor and one receiver is stationary as a master station.
- Ambiguity resolution of carrier phase observations.
- Implementation of a Kalman filter for positioning.
- Heading determination using two receivers on a vehicle.
- Attitude determination using three receivers on a vehicle.
- Master station position estimation applying EGNOS corrections.
- Precise positioning and heading determination using master station and two receivers on a vehicle.
- Precise positioning and attitude determination using master station and three receivers on a vehicle.

## 2.3 Results

Finally, the obtained position accuracy using code and phase observations on carriers L1 and L2 is in the range of a centimeter level . The accuracy of attitude determination reaches below  $0.5^\circ$  level (see Chapter 5). We consider this result quite satisfactory. In a software receiver we did not get higher accuracy compared to code phase observations, however, we believe it could be achieved by implementing a specific PLL loop for precise carrier phase tracking.

# Chapter 3

## Implementation

### 3.1 Coordinate Systems

The WGS 84 Coordinate System is a Conventional Terrestrial Reference System (CTRS). The definitions of this coordinate system are as follows [McC06]:

- It is geocentric, the center of mass being defined for the whole Earth including oceans and atmosphere.
- Its scale is that of the local Earth frame, in the meaning of a relativistic theory of gravitation.
- Its orientation was initially given by the Bureau International de l'Heure (BIH) orientation of 1984.0.
- Its time evolution in orientation will create no residual global rotation with regard to the crust.

The WGS 84 Coordinate System is a right-handed, Earth-fixed orthogonal coordinate system, and is graphically depicted in Figure 3.1.

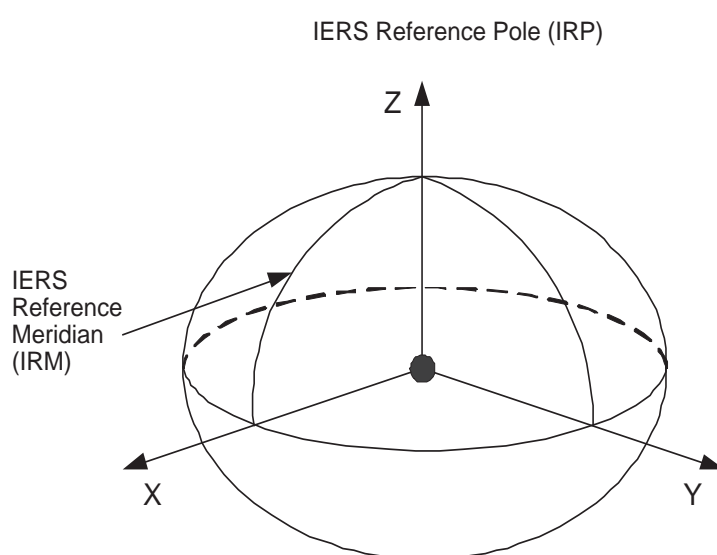


Figure 3.1: The WGS 84 Coordinate System Definition

## CHAPTER 3. IMPLEMENTATION

---

Origin = Earth's center of mass.

Z-Axis = The direction of the IERS Reference Pole (IRP). This direction corresponds to the direction of the BIH Conventional Terrestrial Pole (CTP).

X-Axis = Intersection of the IERS Reference Meridian (IRM) and the plane passing through the origin and normal to the Z-axis. The IRM is coincident with the BIH Zero Meridian.

Y-Axis = Completes a right-handed, Earth-Centered Earth-Fixed (ECEF) orthogonal coordinate system.

The WGS 84 Coordinate System origin also serves as the geometric center of the WGS 84 Ellipsoid and the Z-axis serves as the rotational axis of this ellipsoid.

To achieve a practical realization of a global geodetic reference frame, a set of station coordinates must be established. A consistent set of station coordinates infers the location of an origin, the orientation of an orthogonal set of Cartesian axes, and a scale. A globally distributed set of consistent station coordinates represents a realization of an ECEF Terrestrial Reference Frame (TRF).

The original WGS 84 reference frame established in 1987 was realized through a set of Navy Navigation Satellite System (NNSS) or TRANSIT (Doppler) station coordinates. This frame has been used for GPS since it was established. In 1994 the earth's gravitational constant  $\mu$  was replaced by the standard IERS value, which was established with better accuracy, and the coordinates of the GPS tracking stations were refined. The revised WGS84 came in use from January 2, 1994 and has been given a designation WGS 84 (G730). The "G" indicates that GPS measurements were used to obtain the coordinates and the number 730 denotes the GPS week number when the system was implemented. Another update to the realization of the WGS 84 which was used for GPS since September 29, 1996 is designated as WGS 84 (G873).

The latest realization of the WGS 84 Reference Frame is designated as WGS 84 (G1150). The GPS Operational Control Segment (OCS) implemented it on 20 January 2002. The implementation of improved methodologies has increased the accuracy of the coordinates of the U.S. Air Force (USAF) and National Geospatial-Intelligence Agency (NGA) Global Positioning System monitor stations. The estimated accuracy of WGS 84 (G1150) is on the order of one centimeter (one standard deviation) in each coordinate component for each of the USAF and NGA stations. By comparison, the WGS 84 (G730) and WGS (G873) accuracies were estimated at 10 cm and 5 cm, respectively [Nat06].

## 3.2 Satellite Orbits

The positions of the GPS satellites play the key role in the receiver's position determination. The orbital error influences the accuracy of the measurements. Therefore, the ability to predict the precise position of the satellite is essential for the positioning. With the help of Kepler's laws of planetary motion, ideal elliptical orbits of the GPS satellites can be characterized. The position of a satellite at a given time instant can be calculated from the ephemeris information

included in the navigation message.

### 3.2.1 Keplerian Elements

If all external forces acting on the satellites are neglected the motion of the satellites can be characterized by an elliptical orbit. Actual satellites orbits have the Earth in one of the foci. Six Keplerian elements specify the the shape of the ellipse, the orientation of the orbital plane, and the position of the satellite at any epoch (Figure 3.2). The elements are as follows:

- (a) *semi-major axis* of the ellipse
- (e) *eccentricity* of the ellipse
- (i) *inclination*, the angle between the Earth's equatorial plane and the orbital plane
- (l) *right ascension of the ascending node*, the angle between the direction pointing to the vernal equinox<sup>1</sup> and the ascending node<sup>2</sup>
- ( $\omega$ ) *argument of perigee*, the angle in the plane of the orbit between the ascending node and the perigee (perigee is the point in the satellite orbit when the distance between the center of mass of the Earth and the satellite is the shortest)
- ( $v$ ) *true anomaly*, the angle between the perigee and the satellite position at a specified epoch measured in the orbital plane

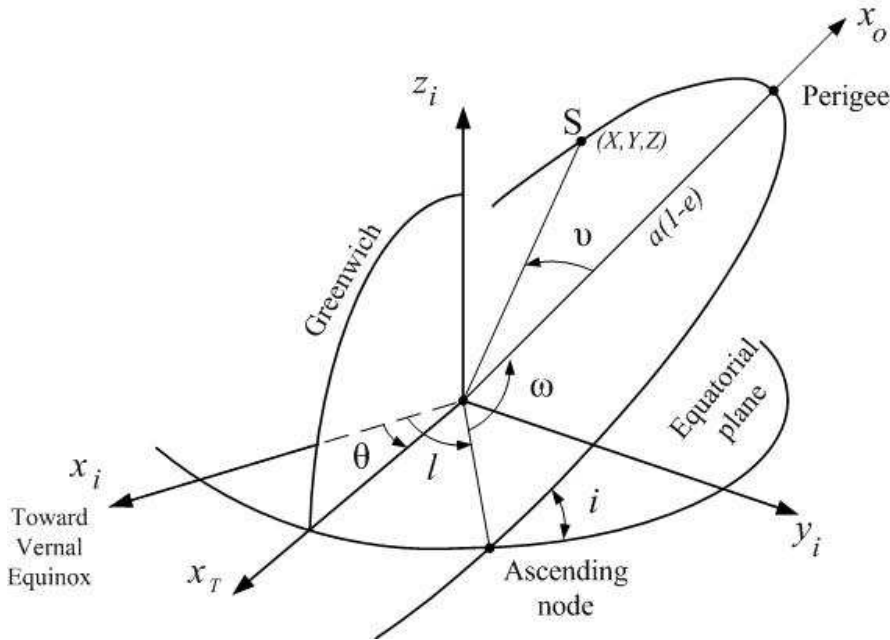
### 3.2.2 Keplerian Motion in Orbital and ECEF Coordinate Systems

In order to determine the location and the velocity of the satellite in the orbital plane the orbital coordinate system is needed (Figure 3.3). The system is defined as follows:

- Origin  $C$  is the center of mass of the Earth,
- $x_o$  axis coincides with the major axis of the orbital ellipse pointing towards the perigee,
- $y_o$  axis is parallel to the minor axis of the ellipse crossing through the focus,
- $z_o$  axis is defined perpendicularly to the  $(x_o, y_o)$  plane completing a right-handed coordinate system.

<sup>1</sup>The point at which the ecliptic (the Earth orbit around the Sun) intersects the Earth's equatorial plane when the sun moving northward.

<sup>2</sup>The point where the satellite orbit rises above the equatorial plane.


 Figure 3.2: Elements of the Keplerian orbits ( $a, e, i, l, \omega, v$ )

Satellite  $S$  moves in the orbital plane. Therefore, there is no need to show  $z_o$  axis. The position vector is denoted by  $\vec{r}$  and the velocity vector is  $\dot{\vec{r}} = d\vec{r}/dt$ . The vectors can be represented by means of true as well as eccentric anomaly. There are three commonly used anomalies of the Keplerian orbits. True  $v(t)$  and eccentric  $E(t)$  anomalies are geometrically producible while mean anomaly  $M(t)$  is an abstract quantity (Figure 3.3). Position  $\vec{r}$  can be found as follows [Lei04]

$$\vec{r} = \begin{bmatrix} X' \\ Y' \\ Z' \end{bmatrix} = \|\vec{r}\| \begin{bmatrix} \cos v \\ \sin v \\ 0 \end{bmatrix} = a \begin{bmatrix} \cos E - e \\ \sqrt{1 - e^2} \sin E \\ 0 \end{bmatrix} \quad (3.1)$$

where magnitude  $\|\vec{r}\|$  is computed as

$$\|\vec{r}\| = \frac{a(1 - e^2)}{1 + e \cos v} = a(1 - e \cos E) \quad (3.2)$$

The mean angular satellite velocity or the mean motion with period of revolution  $P$  follows from Kepler's Third Law<sup>3</sup>

$$n = \frac{2\pi}{P} = \sqrt{\frac{\mu}{a^3}} \quad (3.3)$$

where  $\mu$  is the Earth's gravitational constant.

---

<sup>3</sup>The squares of the orbital periods of planets are directly proportional to the cubes of the semi-major axis of the orbits ( $P^2 \propto a^3$ ).

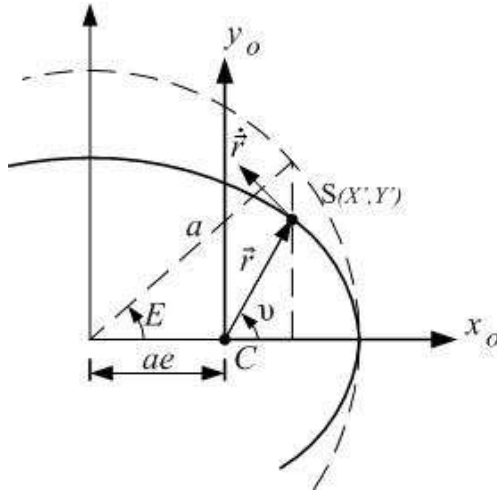


Figure 3.3: Elliptic Keplerian orbit

Navigation message transmitted by the GPS satellites contains the mean anomaly. In order to find the position of the satellite, the true anomaly is needed. There is no straightforward way to obtain the true anomaly from the mean anomaly. Therefore, the eccentric anomaly should be introduced first. The mean and eccentric anomaly are related by Kepler's equation:

$$E = M + e \sin E \quad (3.4)$$

This equation can be solved iteratively. Now from equation (3.1) the true anomaly can be obtained as:

$$v = \arctan \frac{\sqrt{1 - e^2} \sin E}{\cos E - e} \quad (3.5)$$

In equation (3.1) the satellite position is obtained in the orbital plane. In order to find the user position on the globe the satellite coordinates have to be transformed to the (ECEF) coordinate system. The transformation is done by means of direction cosine matrices. First matrix rotates the perigee to the ascending node in the negative direction of  $\omega$ .

$$R(\omega) = \begin{bmatrix} \cos \omega & -\sin \omega & 0 \\ \sin \omega & \cos \omega & 0 \\ 0 & 0 & 1 \end{bmatrix} \quad (3.6)$$

By means of the next matrix the orbit plane changes to the equator plane in the negative direction of the rotate angle  $i$ .

$$R(i) = \begin{bmatrix} 1 & 0 & 0 \\ 0 & \cos i & -\sin i \\ 0 & \sin i & \cos i \end{bmatrix} \quad (3.7)$$

## CHAPTER 3. IMPLEMENTATION

---

For the next transformation it is necessary to introduce the earth-centered inertia (ECI) reference frame. The origin of the ECI frame is at the earth's center of mass. In this frame the z-axis is perpendicular to the equatorial plane and the x-axis is the vernal equinox and in the equator plane. This frame does not rotate with the earth.

Next the ascending node is moved to the vernal equinox. The rotation is done to the negative direction of  $l$ .

$$R(l) = \begin{bmatrix} \cos l & -\sin l & 0 \\ \sin l & \cos l & 0 \\ 0 & 0 & 1 \end{bmatrix} \quad (3.8)$$

The final direction cosine matrix would transform the satellite coordinates from (ECI) to (ECEF) reference frame. But the same result is obtain by substituting another rotation angle: longitude of the ascending node  $\Omega$  in the equation (3.23).

$$\Omega = \Theta - l \quad (3.9)$$

where  $\Theta$  is the Greenwich sidereal time which can be expressed in terms of earth rotation rate  $\omega_e$  and time  $t_s$  elapsed since the Greenwich meridian crossed the vernal equinox as:

$$\Theta = \omega_e t_s \quad (3.10)$$

The resulting position of satellite in ECEF coordinates is calculated as:

$$\begin{bmatrix} X \\ Y \\ Z \end{bmatrix} = R(\Omega) R(i) R(\omega) \begin{bmatrix} \|\vec{r}\| \cos v \\ \|\vec{r}\| \sin v \\ 0 \end{bmatrix} \quad (3.11)$$

### 3.2.3 Satellite Position and Velocity

In case a high accuracy is required, the forces acting on the satellites must be taken into account. The accurate determination of satellite position must consider various disturbing forces. Because of the disturbing forces, the satellite motion deviates from the normal orbit. The disturbances are present because of the shape of the earth, the sun and moon attraction, solar radiation pressure and other forces. Satellites transmit parameters to modify the orbits and they can be obtained from the ephemeris data (Table 3.1).

The following algorithm calculates the satellite position at the time of transmission  $t_{tr}$  [Ser06]. From the ephemeris parameters listed in table (3.1), the semimajor axis  $a$ , the time from ephemeris reference epoch  $t$ , the corrected mean motion  $n$  and the mean anomaly  $M$  are calculated first as:

$$a = (\sqrt{a})^2 \quad (3.12)$$

$$t = t_{tr} - t_{oe} \quad (3.13)$$

Table 3.1: Ephemeris parameters and definitions

Parameter	Explanation	Units
$M_0$	Mean anomaly at reference time	semi-circles
$\Delta n$	Mean motion difference from computed value	semi-circles/sec
$e$	Eccentricity	dimensionless
$\sqrt{a}$	Square root of semi-major axis	$\sqrt{\text{meters}}$
$\Omega_0$	Longitude of ascending node of orbit plane at weekly epoch	semi-circles
$i_0$	Inclination angle at reference time	semi-circles
$\omega$	Argument of perigee	semi-circles
$\Omega_{dot}$	Rate of right ascension	semi-circles/sec
$i_{dot}$	Rate of inclination angle	semi-circles/sec
$C_{uc}$	Amplitude of the cosine correction term to the argument of latitude	rad
$C_{us}$	Amplitude of the sine correction term to the argument of latitude	rad
$C_{rc}$	Amplitude of the cosine correction term to the orbit radius	m
$C_{rs}$	Amplitude of the sine correction term to the orbit radius	m
$C_{ic}$	Amplitude of the cosine correction term to the angle of inclination	rad
$C_{is}$	Amplitude of the sine correction term to the angle of inclination	rad
$t_{oe}$	Ephemeris reference time	sec

$$n = \sqrt{\frac{\mu}{a^3}} + \Delta n \quad (3.14)$$

$$M = M_0 + n t \quad (3.15)$$

The eccentric anomaly  $E$  and the true anomaly  $v$  are obtained from equations 3.4 and 3.5, respectively.

Then the argument of latitude is calculated as:

$$\Phi = v + \omega \quad (3.16)$$

Second harmonic perturbation corrections for argument of latitude  $u$ , radius  $r$  and inclination  $i$  are obtained as:

$$\delta u = C_{us} \sin 2\Phi + C_{uc} \cos 2\Phi \quad (3.17)$$

$$\delta r = C_{rs} \sin 2\Phi + C_{rc} \cos 2\Phi \quad (3.18)$$

$$\delta i = C_{is} \sin 2\Phi + C_{ic} \cos 2\Phi \quad (3.19)$$

Corrected values of argument of latitude  $\Phi$ , radius  $r$  and inclination  $i$  are:

$$u = \Phi + \delta u \quad (3.20)$$

$$r = a(1 - e \cos E) + \delta r \quad (3.21)$$

$$i = i_0 + \delta i + i_{dot} t \quad (3.22)$$

and the corrected longitude of ascending node is

$$\Omega = \Omega_0 + (\Omega_{dot} - \omega_e) t - \omega_e t_{oe} \quad (3.23)$$

Finally coordinates of the satellite in orbital plane can be obtained from

$$\begin{aligned} X' &= r \cos u \\ Y' &= r \sin u \end{aligned} \quad (3.24)$$

and ECEF coordinates are calculated as

$$\begin{aligned} X &= X' \cos \Omega - Y' \cos i \sin \Omega \\ Y &= X' \sin \Omega - Y' \cos i \cos \Omega \\ Z &= Y' \sin i \end{aligned} \quad (3.25)$$

These satellite coordinates are used by a receiver to determine the user location after being compensated for Earth rotation during the signal travel.

Velocity of the satellite is derived as a derivative of the coordinates  $X, Y, Z$  with respect to time.

$$\begin{aligned} \dot{X} &= (\dot{X}' - Y' \dot{\Omega} \cos i) \cos \Omega - (X' \dot{\Omega} + \dot{Y}' \cos i - Y' \frac{\partial i}{\partial t} \sin i) \sin \Omega \\ \dot{Y} &= (\dot{X}' - Y' \dot{\Omega} \cos i) \sin \Omega + (X' \dot{\Omega} + \dot{Y}' \cos i - Y' \frac{\partial i}{\partial t} \sin i) \cos \Omega \\ \dot{Z} &= \dot{Y}' \sin i + Y' \frac{\partial i}{\partial t} \cos i \end{aligned} \quad (3.26)$$

Where

$$\dot{\Omega} = \Omega_{dot} - \omega_e \quad (3.27)$$

is found from equation (3.23),

$$\dot{X}' = \dot{r} \cos u - Y' \dot{u} \quad (3.28)$$

$$\dot{Y}' = \dot{r} \sin u + X' \dot{u} \quad (3.29)$$

are from equation (3.24), and

$$\frac{\partial i}{\partial t} = i_{dot} + 2(C_{is} \cos 2\Phi - C_{ic} \sin 2\Phi) \dot{\Phi} \quad (3.30)$$

is from equations (3.22) and (3.19). Here

$$\dot{\Phi} = \dot{v} = \frac{\dot{E} \sqrt{1 - e^2}}{1 - e \cos E} \quad (3.31)$$

$$\dot{E} = \frac{n}{1 - e \cos E} \quad (3.32)$$

$$\dot{u} = \dot{\Phi} + 2(C_{us} \cos 2\Phi - C_{uc} \sin 2\Phi) \dot{\Phi} \quad (3.33)$$

$$\dot{r} = a e \sin E + 2(C_{rs} \cos 2\Phi - C_{rc} \sin 2\Phi) \dot{\Phi} \quad (3.34)$$

are derived from differentiation of equations (3.5), (3.4), (3.17), (3.20), (3.18), (3.21) with respect to time.

### 3.3 Doppler Effect

The Doppler effect is the apparent change in frequency or wavelength of a wave that is received by an observer moving relatively to the source of the waves. For waves that propagate in a wave medium, the velocity of the observer and the source are reckoned relative to the medium in which the waves are transmitted. The total Doppler effect may, therefore, result from the motion of the source, the motion of the observer, or both. For waves which do not require a medium, such as light or gravity in special relativity only the relative difference in velocity between the observer and the source needs to be considered.

Assume the observer and the source are moving away from each other with a radial velocity  $v$ . Let us consider the problem in the reference frame of the source.

Suppose one wavefront arrives at the observer. The next wavefront is then at a distance  $\lambda = c/f_s$  away from it (where  $\lambda$  is the wavelength,  $f_s$  is the frequency of the source, and  $c$  is the speed of light). Since the wavefront moves with velocity  $c$  and the observer escapes with velocity  $v$ , they will meet after a time

$$T = \frac{\lambda}{c - v} = \frac{1}{(1 - v/c)f_s}$$

Therefore, only velocity in the direction of the source, i.e. radial velocity, influences the time period. However, due to the relativistic time dilation, the observer will measure this time to be

$$T_0 = \frac{T}{\gamma} = \frac{1}{\gamma(1 - v/c)f_s}$$

where  $\gamma = 1/\sqrt{1 - v^2/c^2}$ , so the corresponding frequency is

$$f_0 = \frac{1}{T_0} = \gamma(1 - v/c)f_s = \sqrt{\frac{1 - v/c}{1 + v/c}} f_s$$

When  $v \ll c$ , the approximate expression is

$$\frac{\Delta f}{f_s} = -\frac{v}{c} \quad (3.35)$$

Note, that radial velocity  $v$  is assumed positive when the distance between the source and the observer increases.

## 3.4 Observations in Software Receiver

### 3.4.1 Acquisition

In order to start signal tracking it is necessary to know the precise frequency, carrier and code phases of the signal. Acquisition is used to detect these parameters. Material presented in this section is based on [Kai07].

#### 3.4.1.1 C/A-code Generation

This subsection will describe how to generate C/A-code of GPS satellites. Figure 3.4 shows a shift register structure of C/A-code generator. Both shift registers G1 and G2 have feedbacks

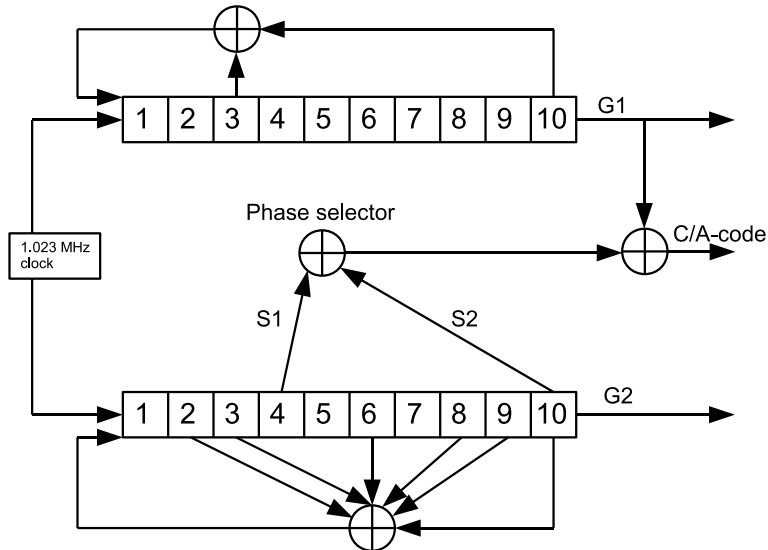


Figure 3.4: C/A-code generation

of modulo-2 combinations of other shift registers. Modulo-2 combination of two G2 registers with the output of G1 produces C/A-code. For every 1023<sup>rd</sup> chip all shift registers are reset to ones. Different combinations of selectors S1 and S2 correspond to different shifts (delays) of G2. Figures 3.5 and 3.6 show autocorrelation of C/A-code with PRN 2 and cross-correlation between PRN codes 2 and 12.

The highest correlation peak appears in case for 0-shift correlation of C/A-code with itself which is a fundamental property.

### 3.4. OBSERVATIONS IN SOFTWARE RECEIVER

---

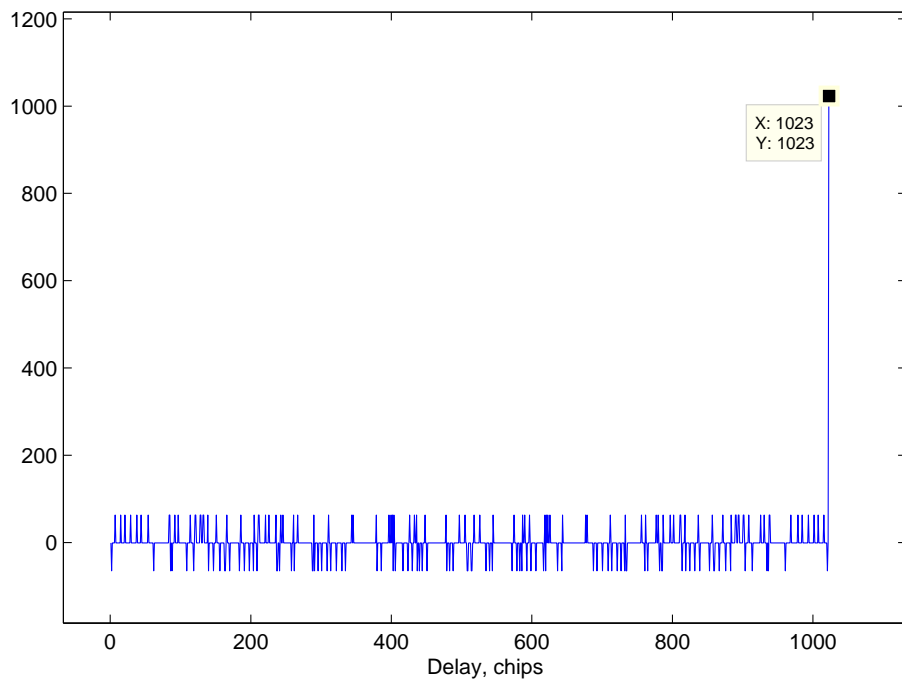


Figure 3.5: Autocorrelation of C/A-code with PRN 2

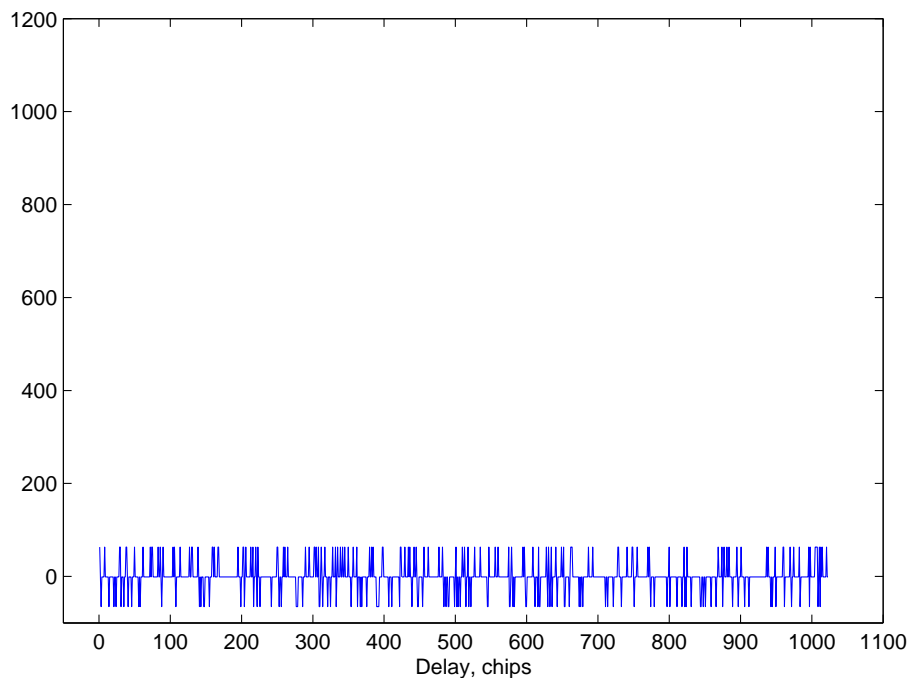


Figure 3.6: Cross-correlation of C/A-codes with PRN 2 and 12

### 3.4.1.2 Estimation of Signal Frequency and Code Phase Shift

Parallel code phase search acquisition is used in order to acquire the satellite signal in our project. The block diagram of this method is shown in Figure 3.7.

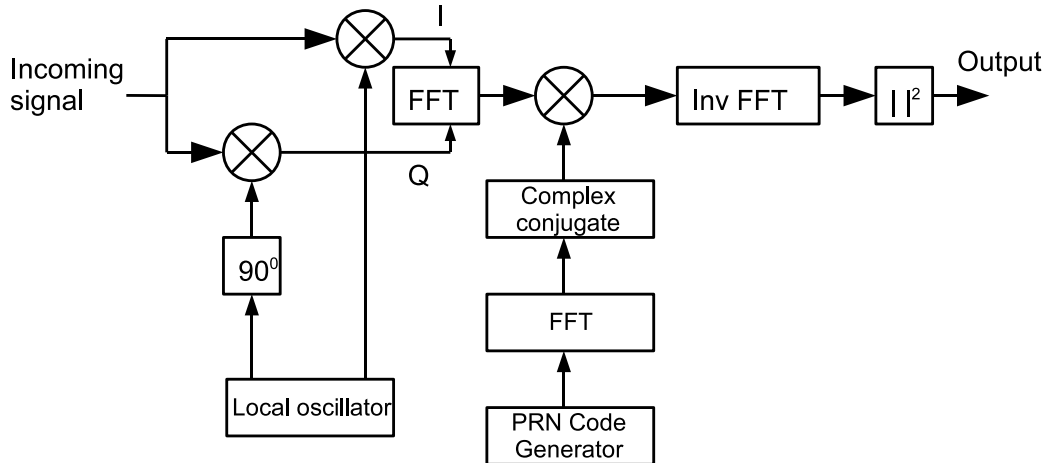


Figure 3.7: Block diagram of parallel code phase search algorithm [Kai07]

One millisecond part of the incoming signal is mixed with a locally generated carrier and its 90° shifted version. A Discrete Fourier Transform (DFT) is taken from the complex combination of the mixers. At the same time Fourier transform of the PRN code is complex conjugated and mixed with the Fourier transform of the other mixers. The result is transformed by inverse Fourier transform, and the output is the absolute value of the result. If a peak is present in the correlation, its index marks the PRN code phase of the incoming signal. The search is done for different frequency bins.

Figure 3.8 presents acquisition results of satellite PRN 26, which has the highest power of the incoming signal. Figure 3.9 shows acquisition results of all GPS satellites: the amplitudes of the peaks are represented as bars. The bars filled by green color indicate acquired satellites. The other low peak amplitudes in the acquisition are due to correlation with noise: the satellite signals are not present.

### 3.4.1.3 Fine Carrier Frequency Resolution

Here 10 millisecond part of the signal is mixed with already detected PRN code (Figure 3.10). Then discrete Fourier transform is taken from the output. The peak in the magnitude of the result corresponds to the carrier frequency of the satellite signal.

Figure 3.11 presents results of fine carrier frequency resolution in acquisition. The accuracy of the determined frequency depends on the length of the DFT. The length corresponds to the number of samples in the analyzed data. Therefore, we use 10 ms data in our project, which provides sufficient accuracy for a tracking loop.

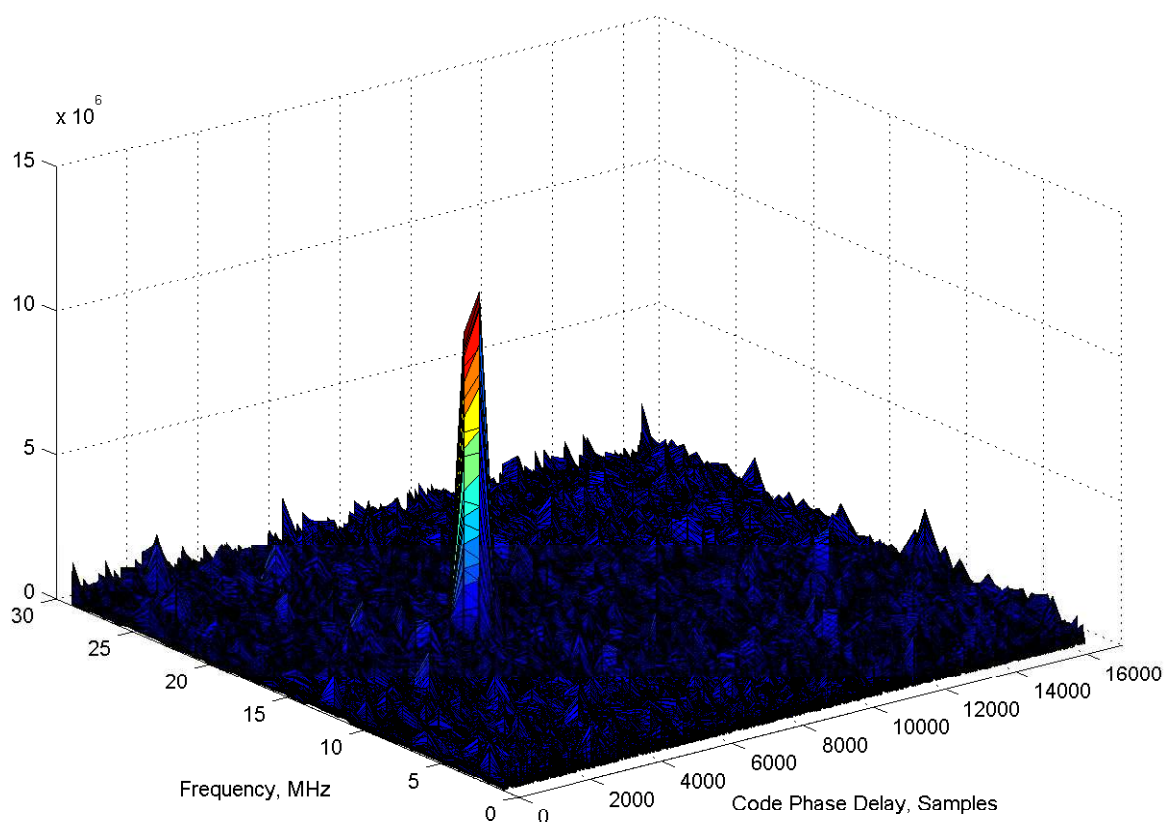


Figure 3.8: Acquisition of EGNOS satellite with PRN 26

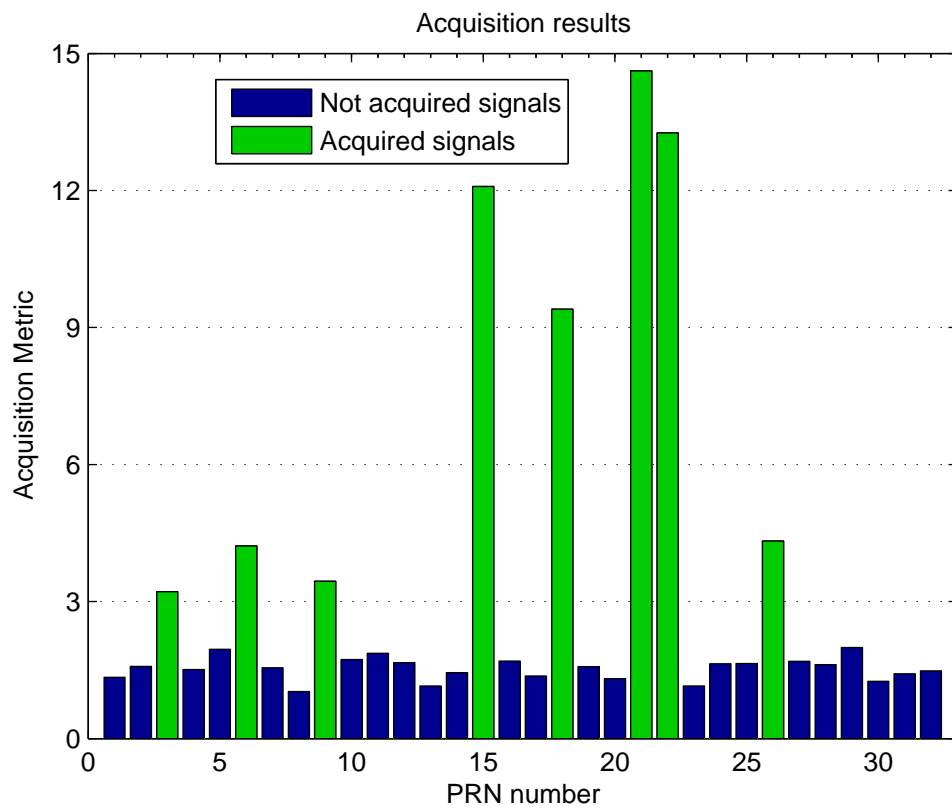


Figure 3.9: Acquisition of all satellites

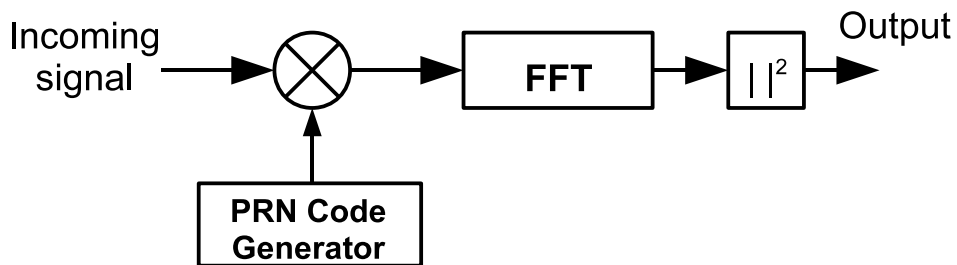


Figure 3.10: Block diagram of parallel frequency space search algorithm [Kai07]

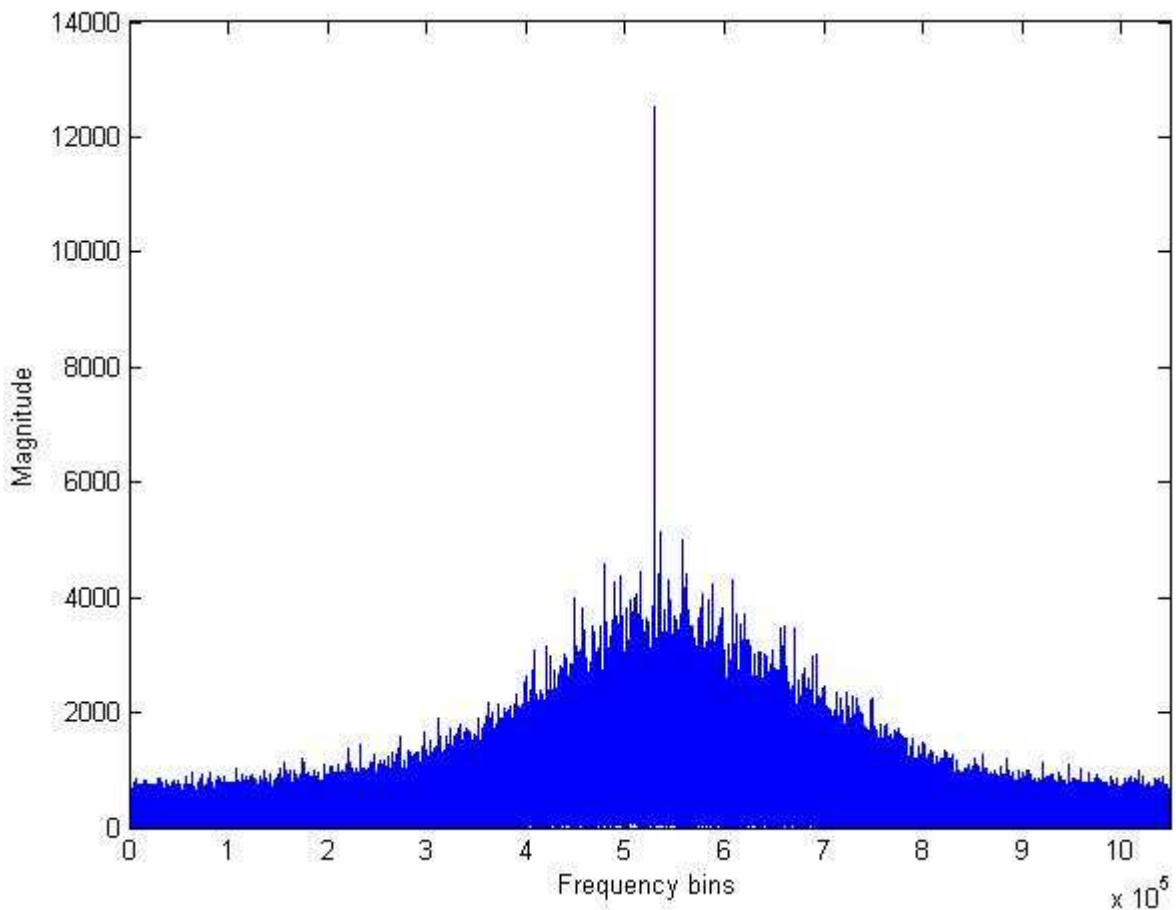


Figure 3.11: Fine carrier frequency estimation

### 3.4.2 Tracking and Data Decoding

The main objective of tracking is to demodulate the data from the signal. In order to get the data from the signal, replicas of a carrier wave and PRN code should be mixed with the incoming signal, furthermore, the replicas must be accurately aligned with the signal. Figure 3.12 shows a block diagram of a tracking channel used in our project.

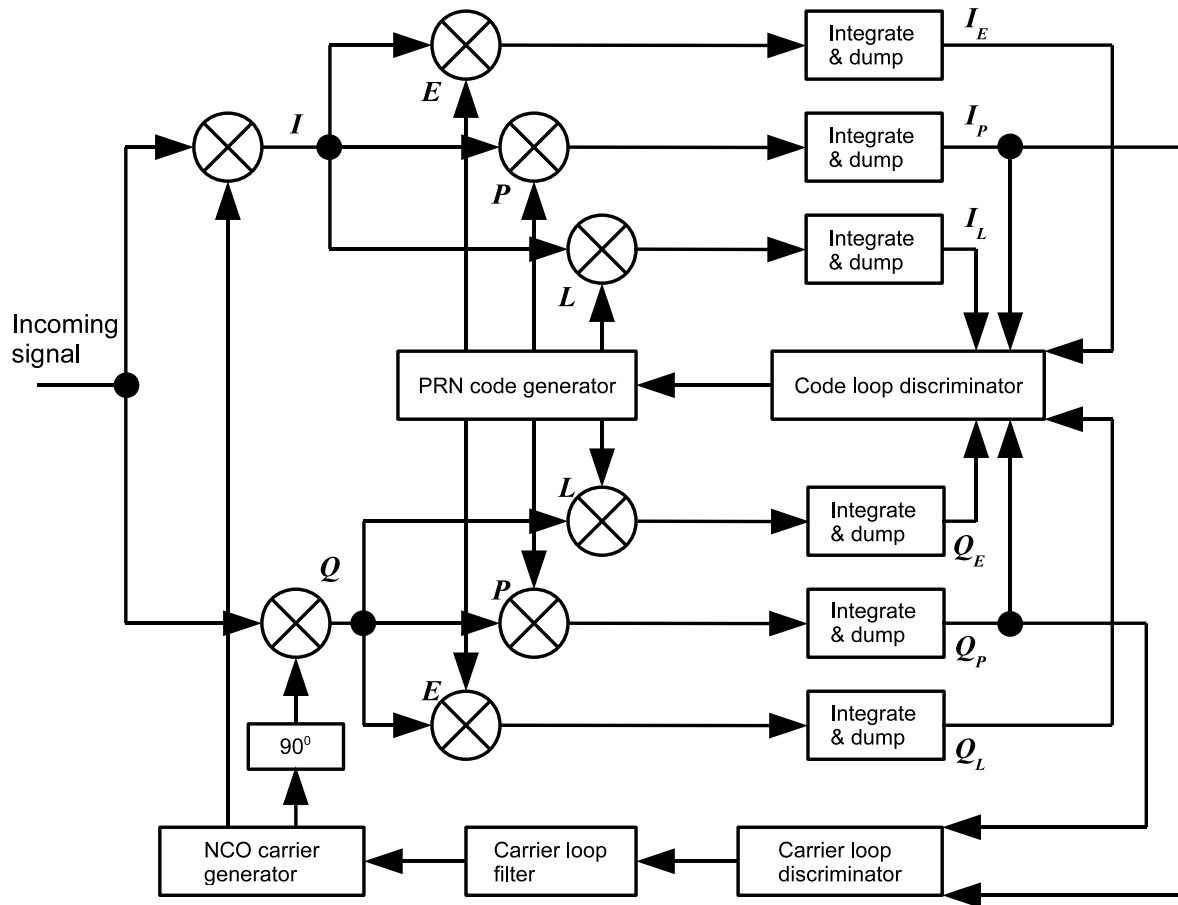


Figure 3.12: Tracking channel [Kai07]

Both a carrier tracking loop (also called as Phase Lock Loop (PLL)) and a code tracking loop (also called as Delay Lock Loop (DLL)) are combined in one block. The task of both loops is to keep track of the incoming signal code and carrier. The initial parameters to generate carrier and code are taken from the acquisition. The PRN code replica to be mixed with the incoming signal comes from the code tracking loop. On the other hand, carrier replica used in the code tracking loop comes from the carrier tracking loop.

Figures 3.13 and 3.14 present tracking results of satellite signal PRN 5. The position concentration around zero indicates a low power in the prompt arm of the tracking channel. This is due to a signal loss of lock. Here the data gets corrupted. There are a few signal losses of lock while tracking the signal.

### 3.4. OBSERVATIONS IN SOFTWARE RECEIVER

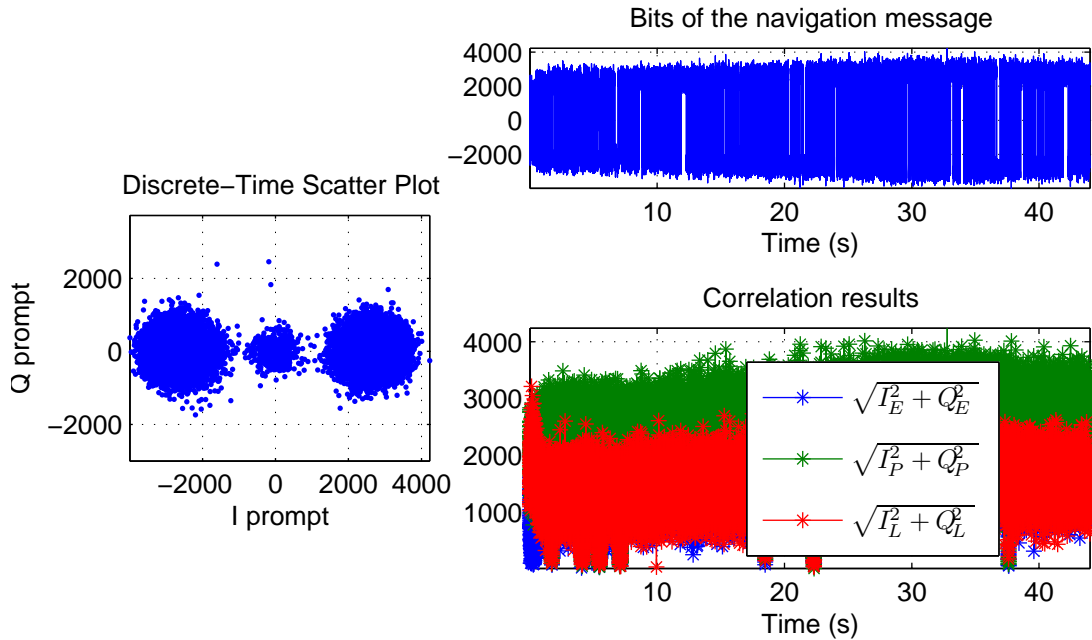


Figure 3.13: Tracking results of satellite PRN 5

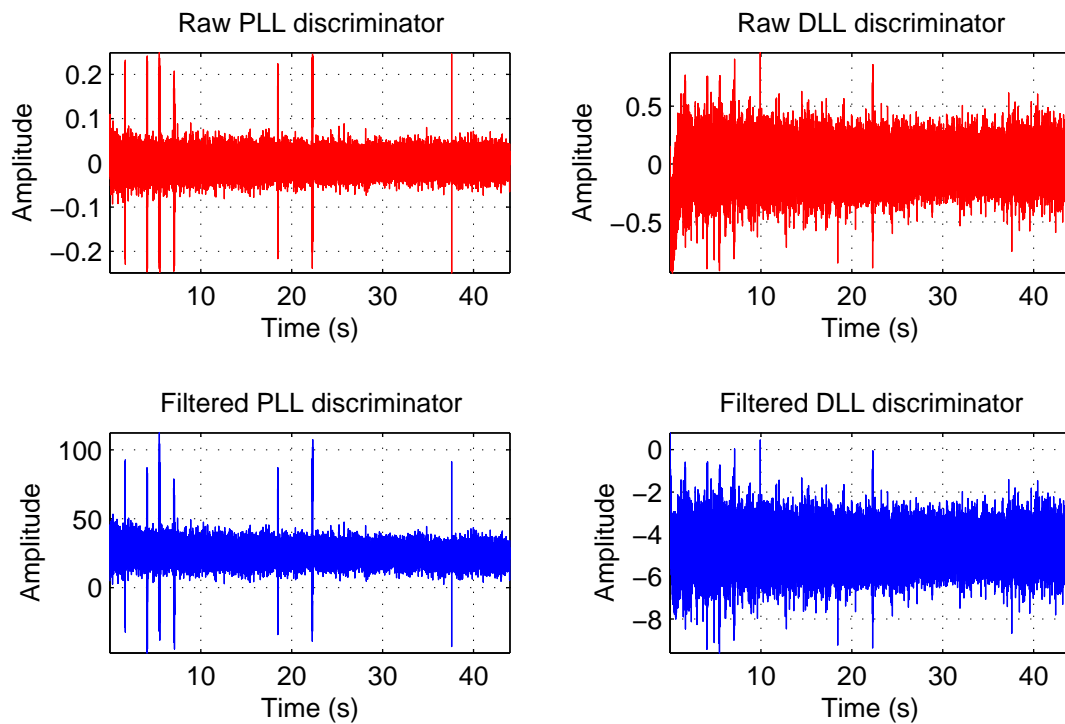


Figure 3.14: PLL and DLL discriminators of tracking satellite PRN 5

### 3.4.3 Code Phase Observations

A pseudorange is an approximate distance from the receiver to a satellite. A code pseudorange between receiver  $i$  and satellite  $k$  measured using the code of carrier L1 is modeled as follows

$$R_i^k = \rho_i^k + I_i^k + T_i^k + c\Delta t_i^k + \epsilon_i^k \quad (3.36)$$

where  $R_i^k$ ,  $\rho_i^k$ ,  $I_i^k$ ,  $T_i^k$ ,  $c\Delta t_i^k$  are pseudorange, true range, ionospheric delay, tropospheric delay, and clock bias between satellite  $k$  and receiver  $i$  scaled to range units. Variable  $\epsilon_i^k$  stands for error, which comes from pseudorange measurements and multipath.

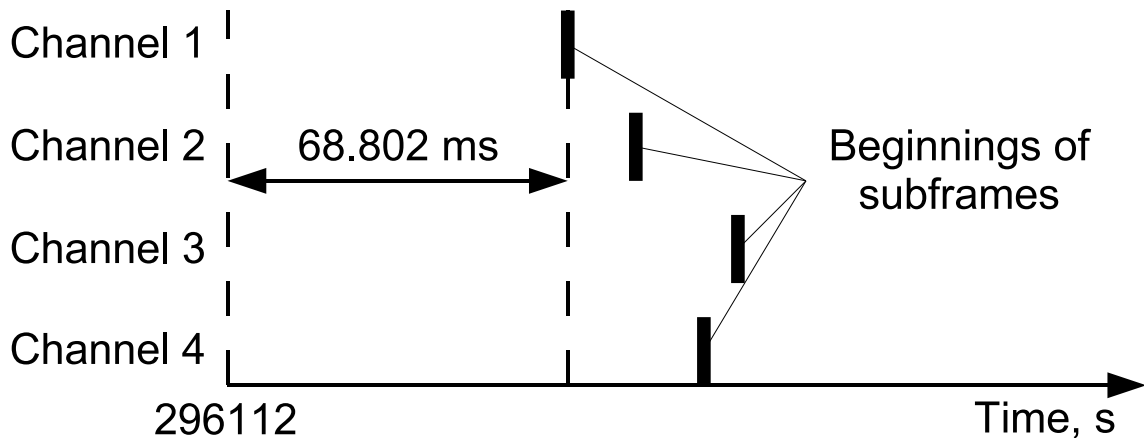


Figure 3.15: Pseudorange measurement

In our software receiver pseudorange measurements are done using the procedure presented in Figure 3.15. A pseudorange to one satellite is set to 68.802 ms and the rest satellite pseudoranges are referenced to it as current sample numbers of the data in the tracking channels are referenced to each other. However, this measurement is ambiguous by one millisecond, which is resolved by the positions of the subframe beginnings in the navigation messages of the satellites. Figure 3.16 depicts results of pseudorange measurements. The reference satellite is satellite PRN 26, therefore, its pseudorange remains constant.

### 3.4.4 Carrier Phase Observations

Besides the code pseudo-range measurements, high precision receivers make phase measurements of the reconstructed carriers. The measured phase consists of integral and fractional components. Fractional component  $\varphi_i(t_0)$  of the phase is a fractional part of the reconstructed carrier at the instant of reception  $t_0$ . Usually it is measured in fractions of cycles or degrees, where 1 cycle or 360 degrees corresponds to the wavelength of the carrier. The standard deviation of such measurement is usually in the range of 2 – 3 mm (about 1 % of the cycle) [Bor97].

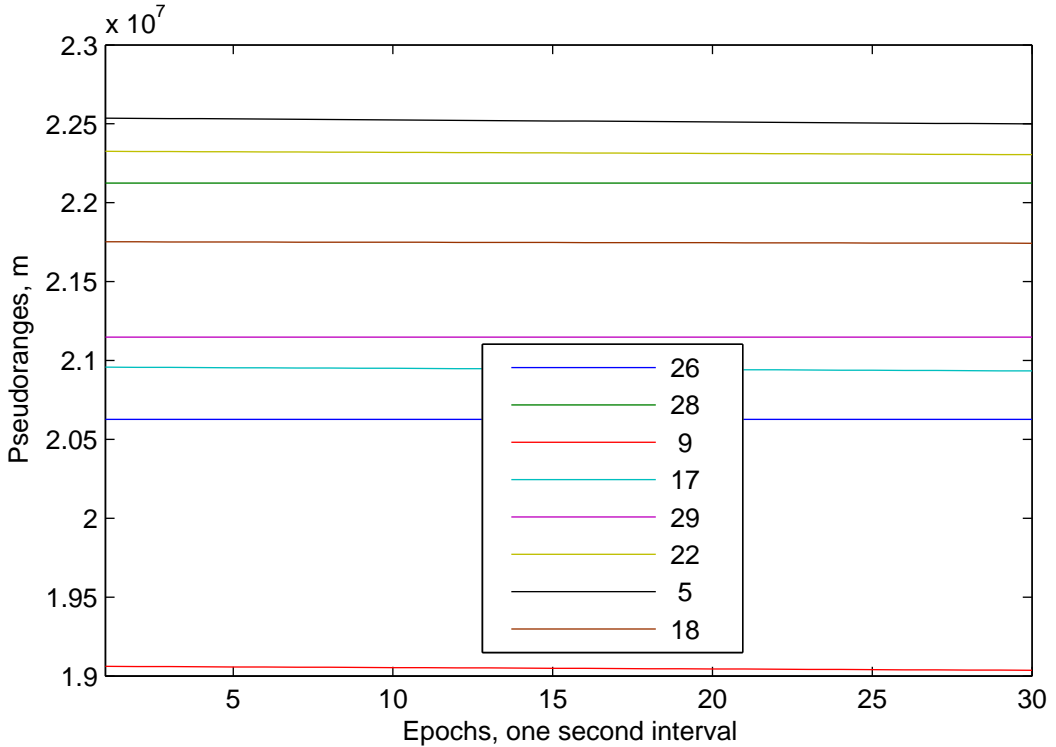


Figure 3.16: Pseudoranges

The integral component is a number of whole wave cycles, which is measured relatively to some initial lock-on value. Receiver-integrated zero-crossing counter registers the number of whole cycles since lock-on moment. The difference between readings of the counter and the number of cycles generated by the local receiver-integrated oscillator corresponds to the change of the range (plus a clock error, as the oscillators are not perfect). Since the initial value is not a true number of cycles between the satellite and the receiver, the phase range is ambiguous. The crucial property of the ambiguity is that as long as there is no loss of signal lock, the ambiguity remains the same and can be resolved. The accuracy of positions based on carrier phase measurements can reach centimeter and sometimes millimeter levels.

GPS signals can be considered as wave packets, since the carriers are modulated. The velocity at which the phase of the pure sinusoidal wave propagates in space is found by the following formula

$$v_{ph} = \lambda \cdot f \quad (3.37)$$

where  $\lambda$  is the wavelength and  $f$  is its frequency.

The total differential of equation (3.37) is valid for any wave

$$dv_{ph} = f d\lambda + \lambda df \quad (3.38)$$

The velocity at which signal energy (information in the case of GPS signals) propagates is

## CHAPTER 3. IMPLEMENTATION

---

defined as a group velocity

$$v_{gr} = \frac{d\omega}{dk} \quad (3.39)$$

where:

$$\omega = 2\pi f \quad (3.40)$$

is the wave's angular frequency, and

$$k = \frac{2\pi}{\lambda} \quad (3.41)$$

is the wave number. Inserting (3.40) and (3.41) into (3.39) can be written as

$$v_{gr} = -\frac{df}{d\lambda} \lambda^2 \quad (3.42)$$

Rearranging equation (3.38) produces

$$\frac{df}{d\lambda} = -\frac{1}{\lambda} \left( f - \frac{dv_{ph}}{d\lambda} \right) \quad (3.43)$$

The substitution of equation (3.43) into (3.42) yields

$$v_{gr} = \frac{1}{\lambda} \left( f - \frac{dv_{ph}}{d\lambda} \right) \lambda^2 = v_{ph} - \frac{dv_{ph}}{d\lambda} \cdot \lambda \quad (3.44)$$

When signals travel through ionosphere their group and phase velocities are not equal because ionosphere is a dispersive medium, i.e. the velocity of wave propagation depends on its frequency [B. 01]

$$v_{ph} = \frac{c}{1 + \frac{k_1}{f^2} + \frac{k_2}{f^3} + \frac{k_3}{f^4} + \dots} \quad (3.45)$$

where  $c$  is the speed of light in vacuum. The coefficients  $k_i$  depend on electron density along the propagation path in the medium.

The wavelength from (3.37) and (3.45) is

$$\lambda = \frac{v_{ph}}{f} = \frac{c}{f + \frac{k_1}{f} + \frac{k_2}{f^2} + \frac{k_3}{f^3} + \dots} \quad (3.46)$$

The squared wavelength is as follows

$$\lambda^2 = \frac{v_{ph}^2}{f^2} = \frac{c^2}{\left( f + \frac{k_1}{f} + \frac{k_2}{f^2} + \frac{k_3}{f^3} + \dots \right)^2} \quad (3.47)$$

Differentiation (3.46) with respect to  $f$  results

$$\frac{d\lambda}{df} = -\frac{c}{\left( f + \frac{k_1}{f} + \frac{k_2}{f^2} + \frac{k_3}{f^3} + \dots \right)^2} \left( 1 - \frac{k_1}{f^2} - 2\frac{k_2}{f^3} - 3\frac{k_3}{f^4} - \dots \right) \quad (3.48)$$

### 3.4. OBSERVATIONS IN SOFTWARE RECEIVER

---

Inserting (3.47) and (3.48) into (3.42) we can find the group velocity of the wave

$$v_{gr} = \frac{c}{1 - \frac{k_1}{f^2} - 2\frac{k_2}{f^3} - 3\frac{k_3}{f^4} - \dots} \quad (3.49)$$

With an estimate of  $k_1$  [B. 01]

$$k_1 = -40.3N_e$$

where  $N_e$  is always positive electron density, and cutting off the series expansion, it follows that  $v_{ph} > v_{gr}$ . Furthermore, the signal code is delayed in the ionosphere approximately by the same period of time as the signal phase is advanced. This is a crucial phenomenon in high precision GPS positioning.

Note, troposphere is not dispersive environment, thus the phase and the code are delayed equally.

A phase pseudorange scaled to range units has the following expression

$$P_i^k = \rho_i^k - I_i^k + T_i^k + c\Delta t_i^k + \lambda N_i^k + \varphi^k(t_0) + \varphi_i(t_0) + \varepsilon_i^k \quad (3.50)$$

Here, ambiguous by  $N_i^k$  cycles phase  $P_i^k$  is not delayed but advanced by  $I_i^k$ . Furthermore,  $\lambda$  is the wavelength,  $\varphi^k(t_0)$  is the unknown fractional part of the phase near the satellite at reception, and  $\varepsilon_i^k$  is noise.

Cutting off the series expansion in (3.49) approximate speeds of the signal code on carriers L1 and L2 are as follows

$$v_{gr1} = \frac{c}{1 - \frac{k_1}{f_1^2}} \quad (3.51)$$

$$v_{gr2} = \frac{c}{1 - \frac{k_1}{f_2^2}} \quad (3.52)$$

Differentials of ionospheric delays based on the previous expressions with respect to time are

$$dI_1 = \left( c - \frac{c}{1 - \frac{k_1}{f_1^2}} \right) dt \quad (3.53)$$

$$dI_2 = \left( c - \frac{c}{1 - \frac{k_1}{f_2^2}} \right) dt \quad (3.54)$$

Ratio between the differentials can be simplified to

$$\frac{dI_2}{dI_1} = \frac{c - \frac{c}{1 - \frac{k_1}{f_2^2}}}{c - \frac{c}{1 - \frac{k_1}{f_1^2}}} = \frac{f_1^2 + k_1}{f_2^2 + k_1} \quad (3.55)$$

Neglecting coefficient  $k_1$  and assuming frequencies of the signals to be constant produces a rough approximation of  $I_2$  with respect to  $I_1$

$$I_2 = \frac{f_1^2}{f_2^2} I_1 \quad (3.56)$$

## CHAPTER 3. IMPLEMENTATION

---

Using the above technique the reader can easily verify that the phase advances are related in the same way as (3.56).

In conclusion, the models of pseudorange and carrier phase observations on both carries L1 and L2 are written again

$$R_{i1}^k = \rho_i^k + I_i^k + T_i^k + c\Delta t_i^k + \epsilon_{1i}^k \quad (3.57)$$

$$P_{i1}^k = \rho_i^k - I_i^k + T_i^k + c\Delta t_i^k + \lambda_1 N_{i1}^k + \varphi_1^k(t_0) + \varphi_{1i}(t_0) + \varepsilon_{1i}^k \quad (3.58)$$

$$R_{i2}^k = \rho_i^k + \frac{f_1^2}{f_2^2} I_i^k + T_i^k + c\Delta t_i^k + \epsilon_{2i}^k \quad (3.59)$$

$$P_{i2}^k = \rho_i^k - \frac{f_1^2}{f_2^2} I_i^k + T_i^k + c\Delta t_i^k + \varphi_2^k(t_0) + \varphi_{2i}(t_0) + \lambda_2 N_{i2}^k + \varepsilon_{2i}^k \quad (3.60)$$

In our software receiver carrier phase observations are done using generated carriers based on frequencies produced by the PLL loops in the tracking channels. Furthermore, the carrier frequencies are corrected by ephemeris parameter  $a_1$  as described in [Kap96]. Figure 3.17 shows generated carrier phase by the PLL tracking loop transformed into range dimensions.

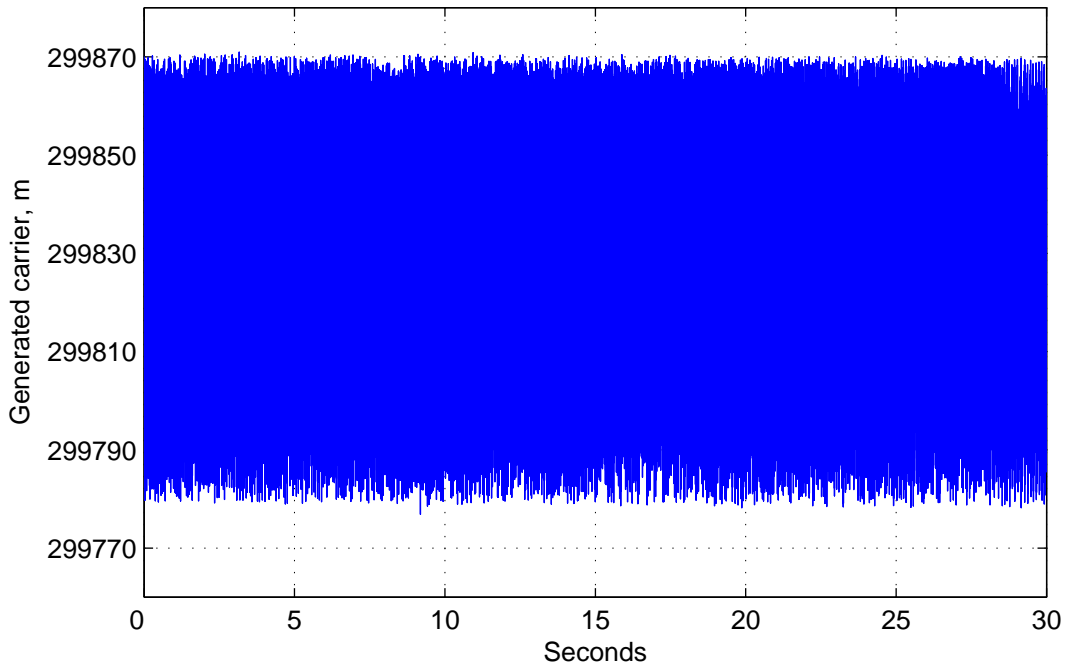


Figure 3.17: Generated carrier based on PLL output frequency

Results of carrier phase measurements obtained from the output of the PLL tracking loops are presented in Figure 3.19.

Positions computed using these carrier phase observations are depicted in Figure 3.18. The carrier phase observations are quite noisy, therefore, the positions have high errors in the range of a few thousand meters.

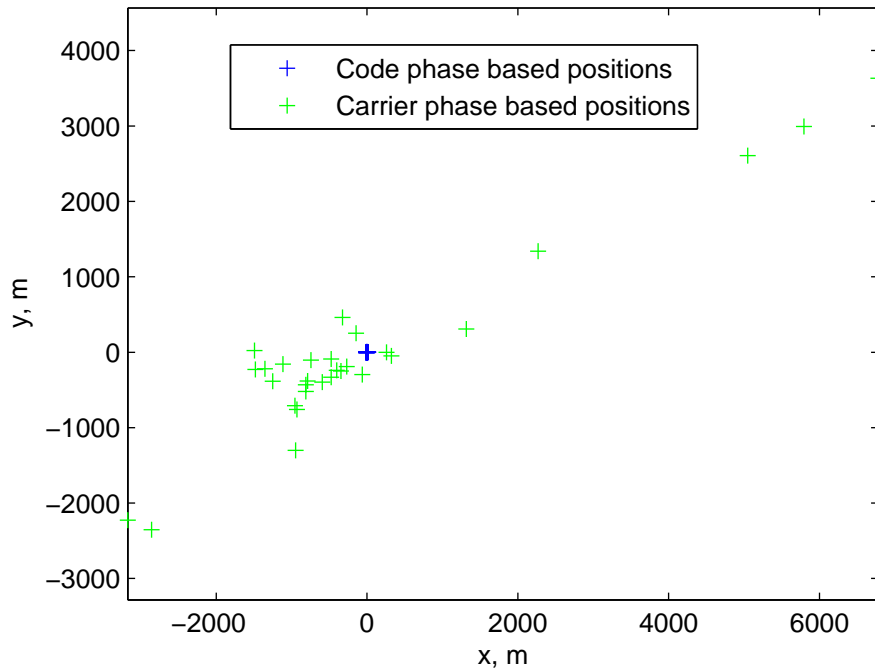


Figure 3.18: Positioning based on code phase and carrier phase observations

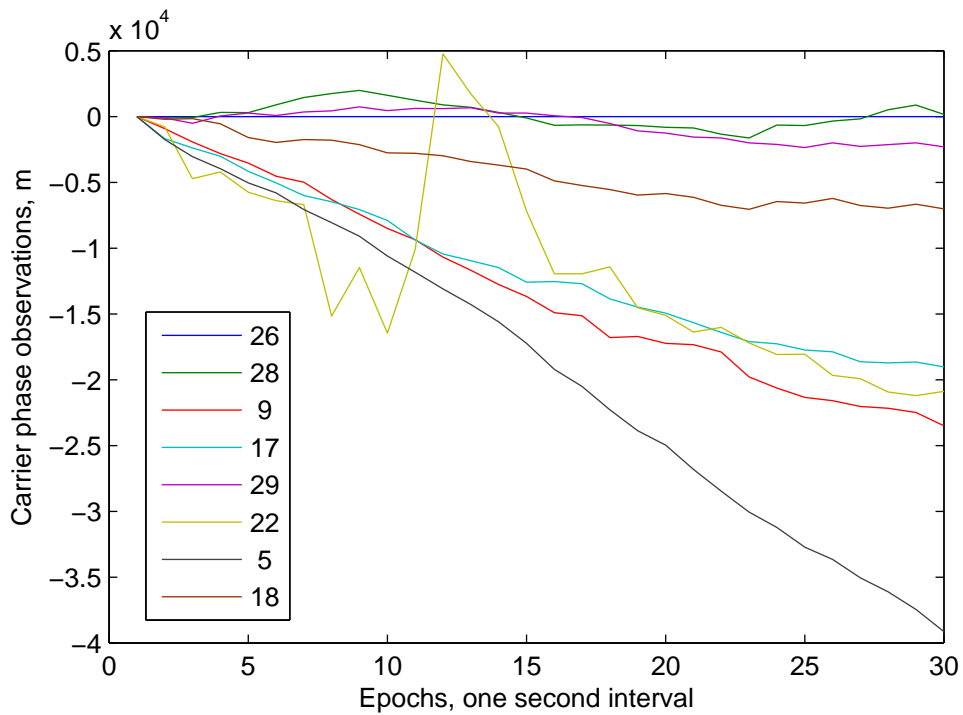


Figure 3.19: Carrier phase observations based on PLL output frequencies

## CHAPTER 3. IMPLEMENTATION

---

It is also possible to generate carriers based on frequencies derived from Doppler shifts according to equation 3.35. Radial velocity  $v$  can be computed using receiver and satellite positions and velocities as follows

$$v = \frac{\vec{P}_{ri} - \vec{P}_s^k}{\|\vec{P}_s^k - \vec{P}_{ri}\|} (\vec{V}_s^k - \vec{V}_{ri}) \quad (3.61)$$

The velocities are in ECEF coordinate system, however, they include the velocity components due to Earth rotation rate.

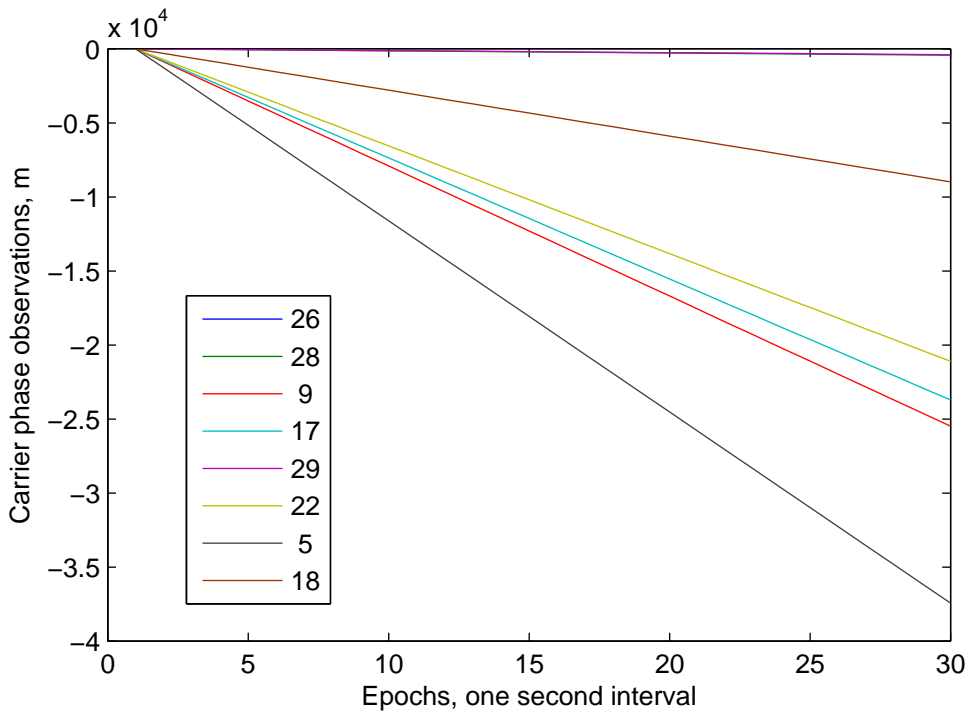


Figure 3.20: Carrier phase observations based on frequencies from satellite velocities

As it is seen from Figures 3.20 and 3.21, the precision of observations and positions is satisfactory now. In conclusion, the problem of carrier phase observations in our software receiver is too noisy PLL tracking loops.

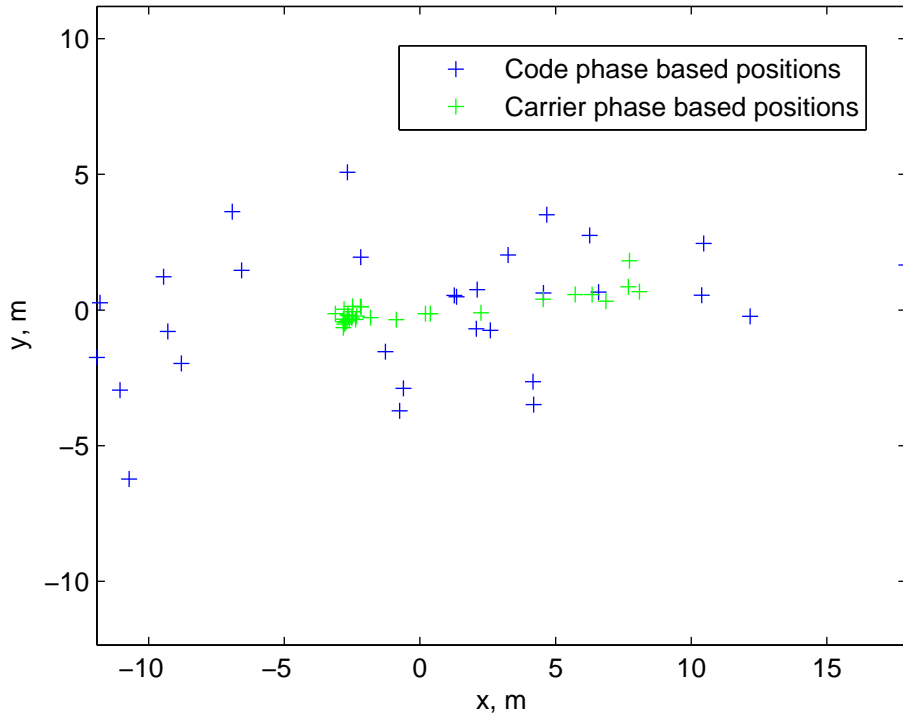


Figure 3.21: Positioning based on code phase and carrier phase observations

## 3.5 Point Positioning

With all known values moved to the left side (noted  $\rho_{rk}^*$ ) the set of observation equations can be written as

$$\begin{cases} \rho_{r1}^* = \sqrt{(X_1 - x)^2 + (Y_1 - y)^2 + (Z_1 - z)^2} + b \\ \dots \\ \dots \\ \rho_{rk}^* = \sqrt{(X_k - x)^2 + (Y_k - y)^2 + (Z_k - z)^2} + b \end{cases} \quad (3.62)$$

Here  $\rho_i^k$  is expanded to  $\sqrt{(X_k - x)^2 + (Y_k - y)^2 + (Z_k - z)^2}$ . The clock offset of the receiver  $c\Delta t_i^k = b$  is common to all equations, because the technique used to measure the signal travel time suffers only from the receiver clock offset, since the clocks of the satellites are highly accurate, stable, and corrected by ephemeris parameters.

In order to solve the set of equations (3.62), the root function is first linearized according to the Taylor model with the first part only being used

$$f(x) = f(x_0) + \frac{f'(x_0)}{1!} \Delta x \quad (3.63)$$

The linearization is expanded with respect to all variables

$$\rho_{rk}^* = \rho_i^k + b + \frac{\partial \rho_{rk}^*}{\partial x} \Delta x + \frac{\partial \rho_{rk}^*}{\partial y} \Delta y + \frac{\partial \rho_{rk}^*}{\partial z} \Delta z + \frac{\partial \rho_{rk}^*}{\partial b} \Delta b \quad (3.64)$$

## CHAPTER 3. IMPLEMENTATION

---

Carrying out partial differentiation results

$$\rho_{rk}^* = \rho_i^k + b - \frac{X_k - x}{\rho_i^k} \Delta x - \frac{Y_k - y}{\rho_i^k} \Delta y - \frac{Z_k - z}{\rho_i^k} \Delta z + \Delta b \quad (3.65)$$

Noting  $\rho_{rk}^* - \rho_i^k - b = omc^k$  produces the set of equations

$$\begin{cases} omc^1 = -\frac{X_1 - x}{\rho_i^1} \Delta x - \frac{Y_1 - y}{\rho_i^1} \Delta y - \frac{Z_1 - z}{\rho_i^1} \Delta z + \Delta b \\ \dots \\ \dots \\ omc^k = -\frac{X_k - x}{\rho_i^k} \Delta x - \frac{Y_k - y}{\rho_i^k} \Delta y - \frac{Z_k - z}{\rho_i^k} \Delta z + \Delta b \end{cases} \quad (3.66)$$

Applying the method of least-squares the system can be solved for  $\Delta x, \Delta y, \Delta z, \Delta b$  with some preliminary value of the receiver position and time bias  $x, y, z, b$ , e.g. zeros. The solution is not weighted because we have no knowledge about the covariance of the observations, therefore, we assume the covariance

$$C_{ob} = \sigma^2 I \quad (3.67)$$

The matrix form of the solution

$$X = (A^T A)^{-1} A^T omc \quad (3.68)$$

After the values  $x, y, z, b$  were improved by  $\Delta x, \Delta y, \Delta z, \Delta b$ , the system of the equations can be solved for  $\Delta x, \Delta y, \Delta z, \Delta b$  again. The process continues until the improvement is negligibly small.

Covariance of the solution is computed according to covariance propagation

$$C_{XX} = \sigma^2 (A^T A)^{-1} \quad (3.69)$$

Usually Dilution of Precision (DOP) is computed as the trace of covariance  $C_{XX}$ . The distribution of satellites above the observer's horizon has a direct effect on the accuracy of the position determination. A low DOP factor is good, a high DOP factor is bad. When satellites are in optimal configuration for a reliable GPS position, the DOP value is low; when they are not, the DOP value is high. If all satellites used for 3-dimensional positioning are crowded together in one part of the sky, the DOP will be high. DOP is like a warning that the actual errors in a GPS position are liable to be larger than you might expect. It is not the errors themselves that are directly increased by the DOP factor, it is the uncertainty of the GPS position that is increased by the DOP factor. There are a number of DOP components: Horizontal Dilution of Precision (HDOP) and Vertical Dilution of Precision (VDOP), when the uncertainty of a solution for positioning has been isolated into its horizontal and vertical components, respectively. When both horizontal and vertical components are combined, the uncertainty of 3-dimensional position is called Position Dilution of Precision (PDOP). In time domain, we have Time Dilution of Precision (TDOP), which indicates the uncertainty of the clock. The combination of all

the above components forms Geometric Dilution of Precision (GDOP). There is also Relative Dilution of Precision (RDOP), that includes the number of receivers, the number of satellites they can handle, the length of the observing session as well as the geometry of the satellites' configuration. Visible satellites, widely and evenly spaced in the sky, indicate good geometry and, therefore, low DOP. Table 3.2 summarizes DOP values [Sic01].

Table 3.2: DOP factors and their implications

Quality	DOP
Very Good	1-2
Good	2-4
Fair	4-5
Suspect	>5

## 3.6 Differential Positioning

It is possible to compute a vector connecting two GPS receivers with considerably higher accuracy than their positions.

Consider Figure 3.22. Basically, in differential positioning a rover position is computed relatively to a master from the projections of the distance between the rover and the master on different directions.

When the receivers are not far away from each other (no more than 40 km) the lines connecting true and broadcasted positions of the satellites with true and computed position of the receivers can be assumed parallel. In this case the dashed parallelograms will be equal, and therefore the baseline (vector connecting the receivers' positions) is not affected by the coordinates of the master position used in the computation of the rover position. In other words, neither the master position with error, nor the accuracy of the satellite position affects the true distance between the rover and the master projected on the direction to the true satellite position. Hence, we have principles of differential positioning.

### 3.6.1 Single Difference of Code Observables

To eliminate the atmospheric effect, equation (3.57) can be differenced as follows

$$R_{ij}^k = \rho_i^k - \rho_j^k + b_{ij} \quad (3.70)$$

Here,  $b_{ij}$  is a differenced clock bias, all the other errors are neglected. To solve the set of equations (3.70) they are linearized according to Taylor model as follows

$$R_{ij}^k = \rho_i^k - \rho_j^k + b_{ij} + \frac{X_k - x}{\rho_j^k} \Delta x + \frac{Y_k - y}{\rho_j^k} \Delta y + \frac{Z_k - z}{\rho_j^k} \Delta z + \Delta b_{ij} \quad (3.71)$$

Position and DOP values are computed in the same way as in point positioning.

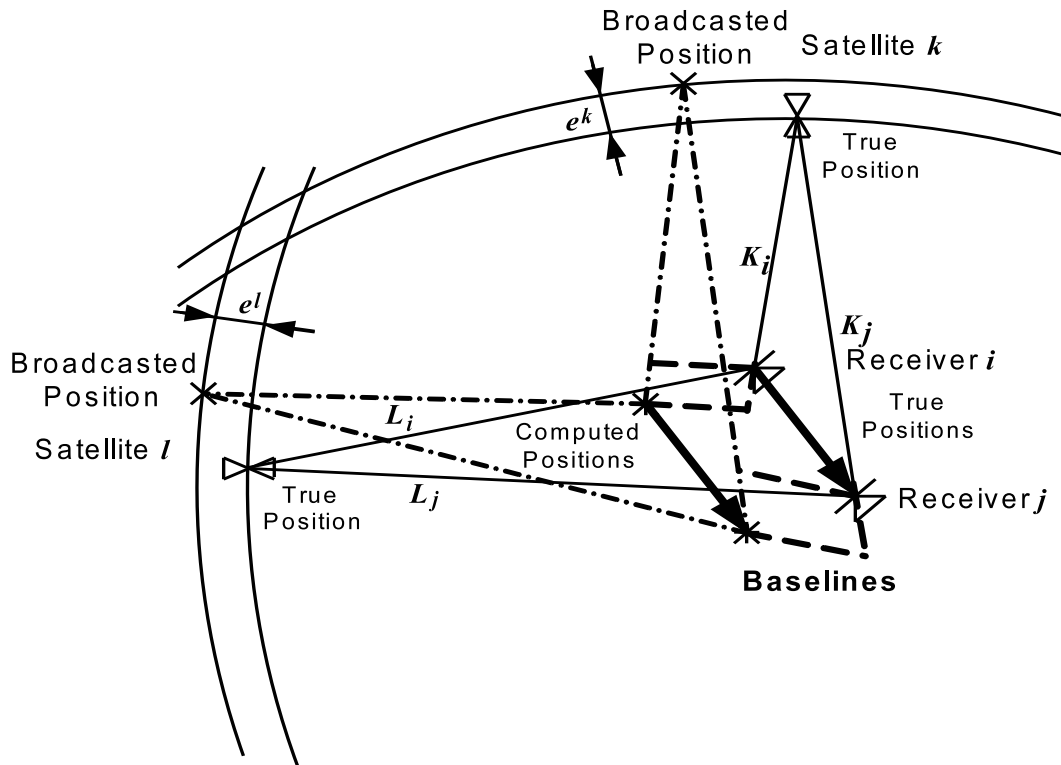


Figure 3.22: Differential positioning

### 3.6.2 Double Difference of Code Observables

To eliminate the atmospheric effect and receivers' clock offsets, equation (3.57) can be differenced as follows

$$R_{ij}^{kl} = \rho_i^k - \rho_i^l - \rho_j^k + \rho_j^l \quad (3.72)$$

All equations should be differenced with reference to satellite  $k$  with the largest elevation angle. When the position of receiver  $i$  is known, the position of receiver  $j$  can be computed from the set of equations (3.72).

First, the equations are linearized according to the Taylor model

$$\begin{aligned} R_{ij}^{kl} = & \rho_i^k - \rho_i^l - \rho_j^k + \rho_j^l + \left( \frac{X_k - x}{\rho_j^k} - \frac{X_l - x}{\rho_j^l} \right) \Delta x + \left( \frac{Y_k - y}{\rho_j^k} - \frac{Y_l - y}{\rho_j^l} \right) \Delta y \\ & + \left( \frac{Z_k - z}{\rho_j^k} - \frac{Z_l - z}{\rho_j^l} \right) \Delta z \end{aligned} \quad (3.73)$$

The position is computed using equation (3.73) in iteration loop starting from some preliminary position. Here, weighted least-squares solution should be used because double differenced observations are correlated.

### 3.6. DIFFERENTIAL POSITIONING

---

The measured observations are not correlated, therefore, we can assume covariance of the observations as

$$C_{ob} = \sigma^2 I \quad (3.74)$$

Double difference is written in a matrix form

$$DD = M \cdot Ob \quad (3.75)$$

Here,

$$M = \begin{bmatrix} 1 & -1 & & -1 & 1 \\ 1 & & -1 & -1 & 1 \\ \vdots & & \ddots & \vdots & \ddots \\ 1 & & & -1 & -1 \\ & & & 1 & \end{bmatrix} \quad (3.76)$$

and

$$Ob = \begin{bmatrix} Ob_i^1 \\ Ob_i^2 \\ \vdots \\ Ob_i^l \\ Ob_j^1 \\ Ob_j^2 \\ \vdots \\ Ob_j^l \end{bmatrix} \quad (3.77)$$

According to covariance propagation

$$C_{DD} = MC_{ob}M^T = \sigma^2 \begin{bmatrix} 4 & 2 & \cdots & 2 \\ 2 & 4 & \cdots & 2 \\ \vdots & \ddots & \ddots & \vdots \\ 2 & 2 & \cdots & 4 \end{bmatrix} \quad (3.78)$$

The weight matrix is the inverse of the covariance [B. 01]

$$W_{DD} = \frac{1}{2\sigma^2(n_{DD} + 1)} \begin{bmatrix} n_{DD} & -1 & \cdots & -1 \\ -1 & n_{DD} & \cdots & -1 \\ \vdots & \ddots & \ddots & \vdots \\ -1 & -1 & \cdots & n_{DD} \end{bmatrix} \quad (3.79)$$

where  $n_{DD}$  is the number of double differenced equations.

The matrix form of the solution is

$$X = (A^T W_{DD} A)^{-1} A^T W_{DD} Ob \quad (3.80)$$

According to the law of covariance propagation, the covariance of the solution (DOP) can be computed according to the following equation

$$C_{XX} = \sigma^2 (A^T W_{DD} A)^{-1} \quad (3.81)$$

### 3.6.3 Double Difference of Phase Observables

Baselines can be computed very accurately when the double differenced pseudoranges are known with high accuracy. Phase pseudoranges are very precise, furthermore, when they are double differenced all errors cancel out except the ambiguities, which have integer nature and are constant over time as long as no loss of signal lock occurs.

One of simple approaches to work with ambiguities is float solution of the combination of code and phase double differenced observations

$$\begin{bmatrix} R_{ij}^{kl} \\ \vdots \\ P_{ij}^{kl} \\ \vdots \end{bmatrix} = \begin{bmatrix} u_{ij}^{k2} & & & & \Delta x \\ u_{ij}^{k3} & & & & \Delta y \\ \vdots & & & & \Delta z \\ u_{ij}^{kl} & 1 & & & \Delta \lambda_1 N_{ij}^{k2} \\ u_{ij}^{k2} & & 1 & & \Delta \lambda_1 N_{ij}^{k3} \\ u_{ij}^{k3} & & & \ddots & \vdots \\ \vdots & & & & \Delta \lambda_1 N_{ij}^{kl} \\ u_{ij}^{kl} & & & & 1 \end{bmatrix} \quad (3.82)$$

Here

$$u_{ij}^{kl} = \left[ \frac{X_k - x}{\rho_j^k} - \frac{X_l - x}{\rho_j^l}; \frac{Y_k - y}{\rho_j^k} - \frac{Y_l - y}{\rho_j^l}; \frac{Z_k - z}{\rho_j^k} - \frac{Z_l - z}{\rho_j^l} \right]$$

Phase observations are a hundred times as precise as code observations. Hence, the weight matrix used in least-squares solution is as follows

$$W_{RP} = \begin{bmatrix} W_{DD} & \\ & 100^2 \cdot W_{DD} \end{bmatrix} \quad (3.83)$$

This method, also called as a float ambiguity resolution, produces positions with accuracy not much better than code double differences. Since the true ambiguities are integers, the float solution should be fixed to integers.

### 3.6.4 Ambiguity Resolution

Ambiguities can be found from double differenced equations (3.57), (3.58), (3.59), (3.60)

$$R_1 = \rho_{ij}^{kl} + \epsilon_{1ij}^{kl} \quad (3.84)$$

$$P_1 = \rho_{ij}^{kl} + \lambda_1 N_{ij1}^{kl} + \varepsilon_{1ij}^{kl} \quad (3.85)$$

$$R_2 = \rho_{ij}^{kl} + \epsilon_{2ij}^{kl} \quad (3.86)$$

$$P_2 = \rho_{ij}^{kl} + \lambda_2 N_{ij2}^{kl} + \varepsilon_{2ij}^{kl} \quad (3.87)$$

### 3.6. DIFFERENTIAL POSITIONING

---

Errors  $\epsilon_{1ij}^{kl}, \epsilon_{2ij}^{kl}$  are in the range of  $\pm(2-3)\text{m}$ , while  $\varepsilon_{1ij}^{kl}, \varepsilon_{2ij}^{kl}$  are in the range of  $\pm(4-6)\text{mm}$  [Eng01].

Rearranged subtraction of divided by  $\lambda_1$  equations (3.85) and (3.87) is as follows

$$60 \cdot \frac{P_1 - P_2}{\lambda_1} = 60N_{ij1}^{kl} - 77N_{ij2}^{kl} + 60 \cdot \frac{\epsilon_{1ij}^{kl} - \epsilon_{2ij}^{kl}}{\lambda_1} \quad (3.88)$$

The error  $60 \cdot \frac{\epsilon_{1ij}^{kl} - \epsilon_{2ij}^{kl}}{\lambda_1}$  is in the range of  $\pm 3$  cycles.

Rearranged subtraction of equations (3.85) and (3.87) divided by  $\lambda_1$  and  $\lambda_2$  (also called as wide lane observation [Eng01]) is as follows

$$\frac{P_1}{\lambda_1} - \frac{P_2}{\lambda_2} = \rho_{ij}^{kl} \left( \frac{1}{\lambda_1} - \frac{1}{\lambda_2} \right) + N_{ij1}^{kl} - N_{ij2}^{kl} + \frac{\epsilon_{1ij}^{kl}}{\lambda_1} - \frac{\epsilon_{2ij}^{kl}}{\lambda_2} \quad (3.89)$$

Insertion of  $\rho_{ij}^{kl}$  from (3.84) into (3.89) yields

$$\frac{P_1}{\lambda_1} - \frac{P_2}{\lambda_2} = R_1 \left( \frac{1}{\lambda_1} - \frac{1}{\lambda_2} \right) + N_{ij1}^{kl} - N_{ij2}^{kl} + \frac{\epsilon_{1ij}^{kl}}{\lambda_1} - \frac{\epsilon_{2ij}^{kl}}{\lambda_2} - \epsilon_{1ij}^{kl} \left( \frac{1}{\lambda_1} - \frac{1}{\lambda_2} \right) \quad (3.90)$$

The error  $\frac{\epsilon_{1ij}^{kl}}{\lambda_1} - \frac{\epsilon_{2ij}^{kl}}{\lambda_2} - \epsilon_{1ij}^{kl} \left( \frac{1}{\lambda_1} - \frac{1}{\lambda_2} \right)$  is in the range of  $\pm 3$  cycles again.

Denoting

$$\begin{cases} K_1 = N_{ij1}^{kl} - N_{ij2}^{kl} \\ K_2 = 60N_{ij1}^{kl} - 77N_{ij2}^{kl} \end{cases} \quad (3.91)$$

$N_{ij1}^{kl}$ , and  $N_{ij2}^{kl}$  can be expressed as

$$\begin{cases} N_{ij1}^{kl} = K_1 + N_{ij2}^{kl} \\ N_{ij2}^{kl} = \frac{60K_1 - K_2}{17} \end{cases} \quad (3.92)$$

All possible values  $K_1$  and  $K_2$

$$\begin{cases} K_1 = \text{round} \left[ \frac{P_1}{\lambda_1} - \frac{P_2}{\lambda_2} - R_1 \left( \frac{1}{\lambda_1} - \frac{1}{\lambda_2} \right) \right] \pm 3 \\ K_2 = \text{round} \left[ 60 \cdot \frac{P_1 - P_2}{\lambda_1} \right] \pm 3 \end{cases} \quad (3.93)$$

can be tested for integer division in equations (3.92), furthermore, the candidates of the ambiguities should meet the range of errors in equations (3.84) and (3.86).

Surprisingly enough such a search produces one or two pairs of candidates: very seldom zero or three pairs are found. All possible combinations of candidates can be tested in position computation, the best matching pairs can be assumed to be the true ones.

This method is insensitive to cycle slips and does not require a stationary receiver, however, it is heavily computational and does not always find all true ambiguities. When cycle slips do not occur often, all candidates produced by the search can be stored in the memory for each epoch, and most frequent pairs can be assumed to be the true ambiguities if the mean of errors  $\epsilon_{1ij}^{kl}, \epsilon_{2ij}^{kl}, \varepsilon_{1ij}^{kl}, \varepsilon_{2ij}^{kl}$  is zero.

## CHAPTER 3. IMPLEMENTATION

---

An alternative is Goad method of ambiguity resolution with use of a Kalman filter. The implementation of the method is based on the example in [Bor97].

The set of double differenced equations (3.57), (3.58), (3.59), (3.60) can be written in a matrix form  $b_k = Ax_k - e_k$  as follows

$$\begin{bmatrix} R_1 \\ P_1 \\ R_2 \\ P_2 \end{bmatrix} = \begin{bmatrix} 1 & 0 & 0 \\ 1 & \lambda_1 & 0 \\ 1 & 0 & 0 \\ 1 & 0 & \lambda_2 \end{bmatrix} \begin{bmatrix} \rho_{ij}^{kl} \\ N_{1ij}^{kl} \\ N_{2ij}^{kl} \end{bmatrix} - \begin{bmatrix} \epsilon_{1ij}^{kl} \\ \varepsilon_{1ij}^{kl} \\ \epsilon_{2ij}^{kl} \\ \varepsilon_{2ij}^{kl} \end{bmatrix} \quad (3.94)$$

The system equation is a steady model  $x_{k|k-1} = x_{k-1|k-1}$ , so the covariance prediction is

$$\Sigma_{k|k-1} = \Sigma_{k-1|k-1} + \Sigma_{\epsilon,k} \quad (3.95)$$

where the transitional covariance matrix  $\Sigma_{\epsilon,k}$  is diagonal

$$\Sigma_{\epsilon,k} = \begin{bmatrix} 10000 & 0 & 0 \\ 0 & 0 & 0 \\ 0 & 0 & 0 \end{bmatrix} \quad (3.96)$$

Such a matrix will give some chance to change  $\rho_{ij}^{kl}$  in  $x$  from epoch to epoch.

Covariance update and Gain matrix are as follows

$$\Sigma_{k|k} = (A\Sigma_{k|k-1}A^T + \Sigma_{\epsilon,k})^{-1} \quad (3.97)$$

$$K_k = \Sigma_{k|k} A^T \Sigma_{k|k-1} \quad (3.98)$$

here,  $\Sigma_{\epsilon,k}$  is the covariance matrix of the observations

$$\Sigma_{\epsilon,k} = \begin{bmatrix} 0.3^2 & 0 & 0 & 0 \\ 0 & 0.005^2 & 0 & 0 \\ 0 & 0 & 0.3^2 & 0 \\ 0 & 0 & 0 & 0.005^2 \end{bmatrix} \quad (3.99)$$

The state update is computed according to the following equation

$$x_{k|k} = x_{k|k-1} + K_k(b_k - Ax_{k|k-1}) \quad (3.100)$$

The corrected covariance matrix prepared for the next epoch

$$\Sigma_{k|k} = (I - K_k A) \Sigma_{k|k-1} \quad (3.101)$$

The process starts from initial values

$$\Sigma_{0|0} = \begin{bmatrix} 10 & 0 & 0 \\ 0 & 10 & 0 \\ 0 & 0 & 10 \end{bmatrix} \quad (3.102)$$

$$x_{1|0} = (A^T A)^{-1} b_0 \quad (3.103)$$

The true ambiguities are found from the combinations based on the set of equations (3.92)

$$K1 = \text{round}(x_{k|k}(2, 1) - x_{k|k}(3, 1)) \quad (3.104)$$

$$K2 = \text{round}(60 * b_k(2, 1) / \lambda_1 - 77 * b_k(4, 1) / \lambda_2) \quad (3.105)$$

$$\text{true}N_2 = \text{round}((60 * K1 - K2) / 17) \quad (3.106)$$

$$\text{true}N_1 = \text{round}(\text{true}N_2 + K1) \quad (3.107)$$

It can be easily seen from equation (3.89) that estimated  $K1 = N_{ij1}^{kl} - N_{ij2}^{kl}$  has much smaller error than  $N_{ij1}^{kl}, N_{ij2}^{kl}$  alone. When  $K1$  is filtered to the correct value, equations (3.106), (3.107) will produce the true ambiguities, since the error in  $K2$  will be reduced by division by 17, and removed completely by rounding. Furthermore, to ensure the removal of the error in  $K2$ , it can be averaged over epochs.

The more epochs are processed, the more correctly  $K1$  is filtered, consequently, the more reliable are the resolved ambiguities.

Goad method works well on average, however, sometimes (especially at the beginning) the resolved ambiguities are not correct. Combination of the search method with Goad's could be a solution.

If the resolved ambiguity is not detected by the search method, it is certainly not the correct one. Then, for the satellite all available candidates (or the most frequent) are tested, and the best is chosen as the true one. If the resolved ambiguity exists in the set of candidates produced by the search method, the probability of it being the true resolution is high, therefore, it is assumed to be the true one.

In many cases of our measurements this combination of the two methods produced the true ambiguities from the first or the second epochs. Consequently, we can conclude that such a combination is not highly computational, and it has a better performance compared to the original Goad method.

### 3.6.5 Cycle Slip Detection and Repair

If a receiver can make integrated Doppler observations, cycle slips can be detected by comparing differences of measured phases with phase differences derived from integrated Doppler which has the advantage of being immune from cycle slips [B. 01].

When there are no cycle slips, the ambiguity remains constant. Difference between the ambiguities on carriers L1 and L2 can be found by differencing equations 3.85 and 3.87.

$$P_1 - P_2 = \lambda_1 N_{ij1}^{kl} - \lambda_2 N_{ij2}^{kl} + \varepsilon_{1ij}^{kl} - \varepsilon_{2ij}^{kl} \quad (3.108)$$

The combined error from carrier phase observations on carriers L1 and L2 is below one centimeter. The lowest jump caused by cycle slips in such differencing is about 5.5 cm (difference

between wavelengths): if the cycle slips on both carrier phase observations L1 and L2 are one cycle. Figure 3.23 presents results for the case when there is no cycle slips. As it can be seen the magnitude of noise is below one centimeter.

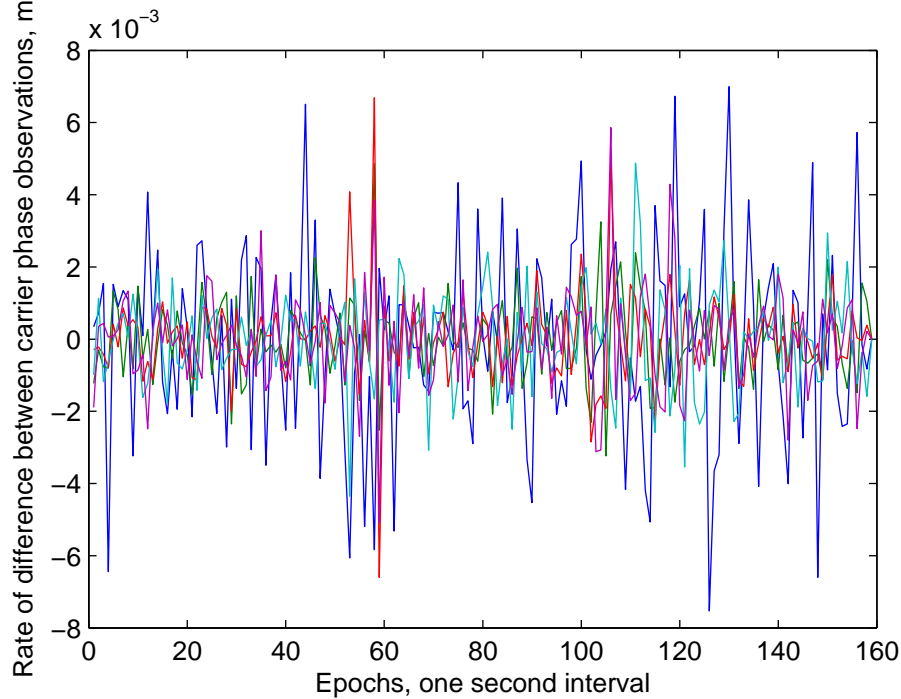


Figure 3.23: Rate of difference between carrier phase observations on L1 and L2 without cycle slips

Figure 3.24 shows results for another receiver. Here high magnitude peaks indicate cycle slips.

In our project if the rate is higher than 5 cm, covariance update matrix  $\Sigma_{k-1,k-1}$  and state update  $x_{x|x-1}$  are reset to the initial values. The information about candidates produced by the "search" method is erased too.

### 3.7 Computing Positions by Kalman Filter

In our project the receivers are fixed to the roof of the tractor. Tractor movement in fields is unpredictable, therefore, as state transition model  $F_{k-1}$  identity matrix is used. To have the least-squares fitted position for all observations we build a Kalman filter as follows.

The state equation is as for a steady model

$$x_k = F_{k-1}x_{k-1} + \epsilon_k \quad (3.109)$$

Covariance  $\Sigma_{\epsilon,k}$  of our system in case of stationary tractor is defined as

### 3.7. COMPUTING POSITIONS BY KALMAN FILTER

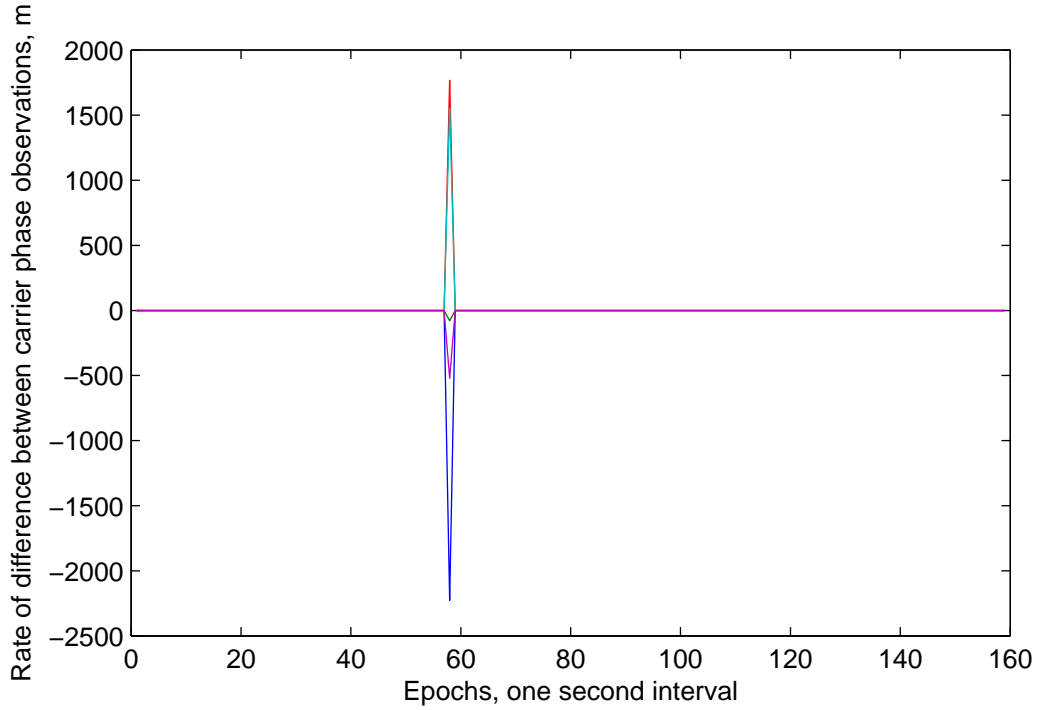


Figure 3.24: Rate of difference between carrier phase observations on L1 and L2 with cycle slips

$$\Sigma_{\epsilon,k} = E\{\epsilon_k \epsilon_k^T\} = \begin{bmatrix} 0.01^2 & 0 & 0 \\ 0 & 0.01^2 & 0 \\ 0 & 0 & 0.01^2 \end{bmatrix} \quad (3.110)$$

and in case of a moving tractor

$$\Sigma_{\epsilon,k} = E\{\epsilon_k \epsilon_k^T\} = \begin{bmatrix} 2^2 & 0 & 0 \\ 0 & 2^2 & 0 \\ 0 & 0 & 2^2 \end{bmatrix} \quad (3.111)$$

Equation of observations can be written as

$$b_k = A_k x_k + e_k \quad (3.112)$$

with the inverse of observation covariance

$$\Sigma_{e,k} = 0.03^2 \begin{bmatrix} 4 & 2 & \dots & 2 \\ 2 & 4 & \dots & 2 \\ \vdots & \ddots & \ddots & \vdots \\ 2 & 2 & \dots & 4 \end{bmatrix}^{-1} \quad (3.113)$$

Observations are double differenced using a reference satellite with the largest elevation angle.

## CHAPTER 3. IMPLEMENTATION

---

The process starts from the preliminary position computed by least-squares solution, therefore, the covariance of the state vector starts from the following initial value

$$P_{0|0} = \begin{bmatrix} 1 & 0 & 0 \\ 0 & 1 & 0 \\ 0 & 0 & 1 \end{bmatrix} \quad (3.114)$$

Predicted covariance

$$P_{k|k-1} = F_{k-1} P_{k-1|k-1} F_{k-1}^T + \Sigma_{\epsilon,k} \quad (3.115)$$

Kalman gain matrix

$$K_k = P_{k|k-1} A_k^T (A_k P_{k|k-1} A_k^T + \Sigma_{e,k})^{-1} \quad (3.116)$$

Correction is found according to the following formula

$$x_{k|k} = x_{k|k-1} + K_k (b_k - A_k x_{k|k-1}) \quad (3.117)$$

Here  $b_k$  are double differenced carrier phase observations with which include already resolved ambiguity resolution,  $x$  is a baseline vector. Matrix  $A_k$  is computed as follows

$$A_k = \begin{bmatrix} \frac{X_k-x}{\rho_j^k} - \frac{X_1-x}{\rho_j^1} & \frac{Y_k-y}{\rho_j^k} - \frac{Y_1-y}{\rho_j^1} & \frac{Z_k-z}{\rho_j^k} - \frac{Z_1-z}{\rho_j^1} \\ \vdots & & \\ \frac{X_k-x}{\rho_j^l} - \frac{X_l-x}{\rho_j^l} & \frac{Y_k-y}{\rho_j^l} - \frac{Y_l-y}{\rho_j^l} & \frac{Z_k-z}{\rho_j^l} - \frac{Z_l-z}{\rho_j^l} \end{bmatrix} \quad (3.118)$$

Then, the covariance is updated as

$$P_{k|k} = (I - K_k A_k) P_{k|k-1} \quad (3.119)$$

## 3.8 Attitude Determination

### 3.8.1 Background

GPS can provide attitude information even though it was originally developed for navigation purposes. With high precision of carrier phase measurements it is possible to determine relative positions of antennas mounted on a vehicle.

Attitude determination with GPS and multiple antennas is based on the principle shown in Figure 3.25. The signal wavefront can be considered planar when it arrives to the antennas because the distance between GPS antennas is much smaller as compared to the distance to GPS satellites. It is quite unlikely that the baseline between the antennas will be perpendicular to the line of sight to the satellite. The signal will first reach the closer antenna and little later the distant one. By measuring the difference in carrier phase between the antennas it is possible to determine a relative range between a pair of antennas projected on the line of sight between

the receivers and the satellite. With a minimum of three antennas it is possible to estimate three dimensional attitude of an object. This approach is used in attitude determination receivers.

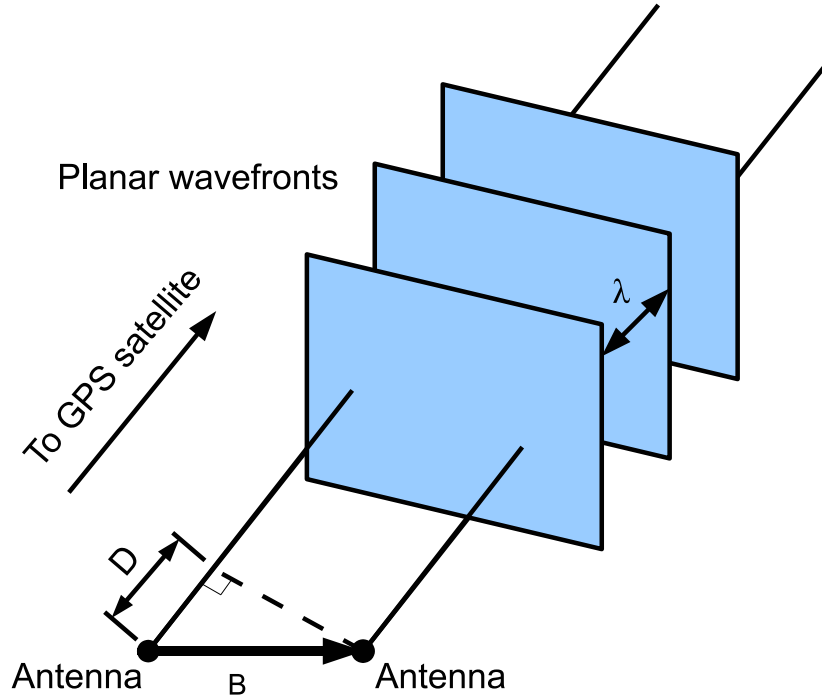


Figure 3.25: Attitude geometry. Courtesy of [Jam96]

### 3.8.2 Coordinate Frame Definition

In attitude determination a vehicle is defined in two separate reference frames: the local horizontal coordinate system and a vehicle body coordinate system. Both coordinate systems are right-handed.

Coordinate frames and rotation angles are defined as shown in Figure 3.26. The axes of the local horizontal frame are defined in the way that the  $y$  axis points to the north,  $x$  axis points to the east, and  $z$  axis points upward along the local vertical completing the right-handed set of axes. The body reference frame is fixed to the vehicle with  $y'$  axis pointing to the front,  $x'$  axis pointing to the right side of the vehicle and  $z'$  completes the right handed coordinate axis set by pointing upward.

The rotation around  $y$  axis is called *roll*, while the rotation around  $x$  axis is called *pitch*, and *yaw* is the rotation around vertical  $z$  axis. When roll, pitch, and yaw angles are all zero, the body frame is aligned with local horizontal frame. Starting from this reference position, the body frame is first rotated around  $z$  axis by heading angle  $\psi$ . Then, the body frame is rotated around the new pitch axis by pitch angle  $\theta$ . Finally, the it is rotated around roll axis by roll angle  $\varphi$ . All rotations are in positive directions, right-handed sense.

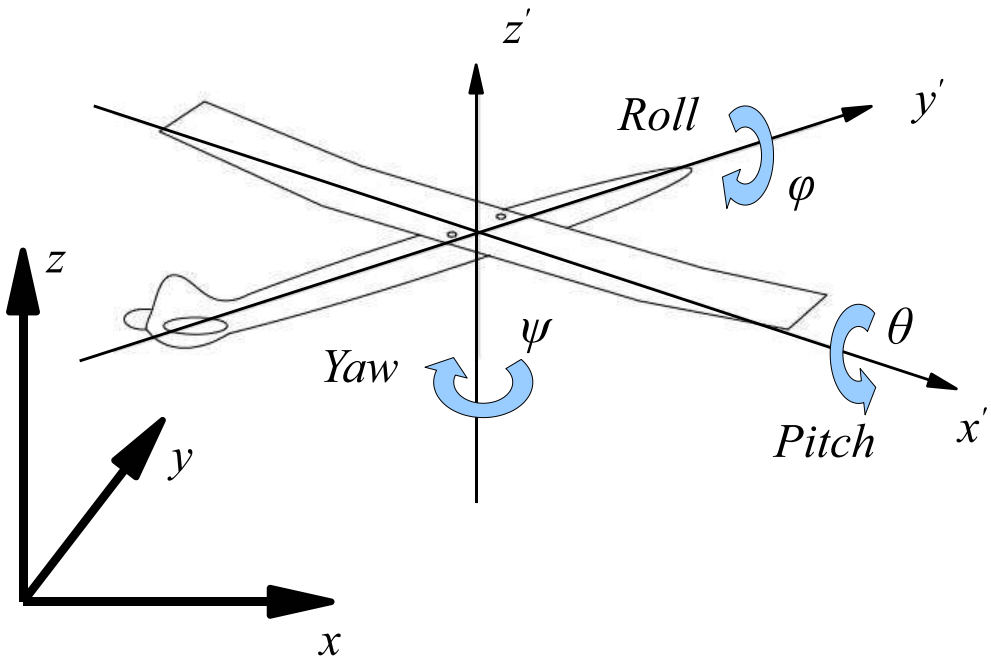


Figure 3.26: Coordinate frames and rotation angles

### 3.8.3 System Setup

To be able to measure all three rotation angles and have a good position accuracy we built the following system: one Ashtech Z-Xtreme GPS receiver was positioned on a field with a stationary antenna, two Topcon Legasy-E receivers and another Ashtech Z-Xtreme receiver were placed in a tractor with their antennas located on the tractor roof as shown in Figure 3.27.

The placement of the antennas represents an equilateral triangle with the side length of two meters.

### 3.8.4 Roll, Pitch, and Yaw Determination

To estimate an attitude of a vehicle, the coordinates of mounted GPS antennas have to be known. Coordinates  $X, Y, Z$  of GPS antennas have to be transformed from ECEF coordinate system into Universal Transverse Mercator (UTM) coordinate system in order to obtain Easting, Northing, and Upping. Having UTM coordinates, angles roll, pitch, and yaw can be determined relatively to the local horizontal plane.

All three angles are important to know for a flying vehicle (airplane etc.). If the vehicle moves on the ground, it is often enough to know only its heading. For the heading determination only two antennas are necessary. Depending on the number of antennas, Tait-Bryan angles can be determined differently. For the testing porpoises we used different constellation of antennas. The methods for the angle determination with different available antennas are presented further.



Figure 3.27: Location of GPS antennas on a vehicle

The attitude determination begins from heading. To determine yaw, we have to consider the antennas in plane P1 parallel to the local horizontal plane (Figure 3.28). Two Topcon antennas, represented in the figure by the marks B and C, are used in heading determination. Angle yaw is calculated as:

$$\psi = \arcsin \left( \frac{\|\overrightarrow{KB}\|}{\|\overrightarrow{CB}\|} \right) \quad (3.120)$$

In case of three available antennas the precision of yaw determination is improved by taking mean of yaw computations using two different pairs of antennas. Both angles are calculated according to equation 3.120, however, the coordinates of point B are different. These coordinates are known from the position computation. Furthermore, the coordinates of point B can be found using already known geometry of the antennas, coordinates of points A and C.

In our project the following approach is implemented. Distances between the antennas are expressed through the coordinates of the positions with known values at the left side

$$\begin{cases} D_{BC}^2 - (u_B - u_C)^2 = (e_B - e_C)^2 + (n_B - n_C)^2 \\ D_{AB}^2 - (u_B - u_A)^2 = (e_B - e_A)^2 + (n_B - n_A)^2 \end{cases} \quad (3.121)$$

Here  $D_{BC}$  and  $D_{AB}$  are distances between antennas A, B, and C. Variables  $e$ ,  $n$ ,  $u$  stand for UTM coordinates of the antennas. Position coordinates of point B  $u_B$  and  $e_B$  are assumed unknown.

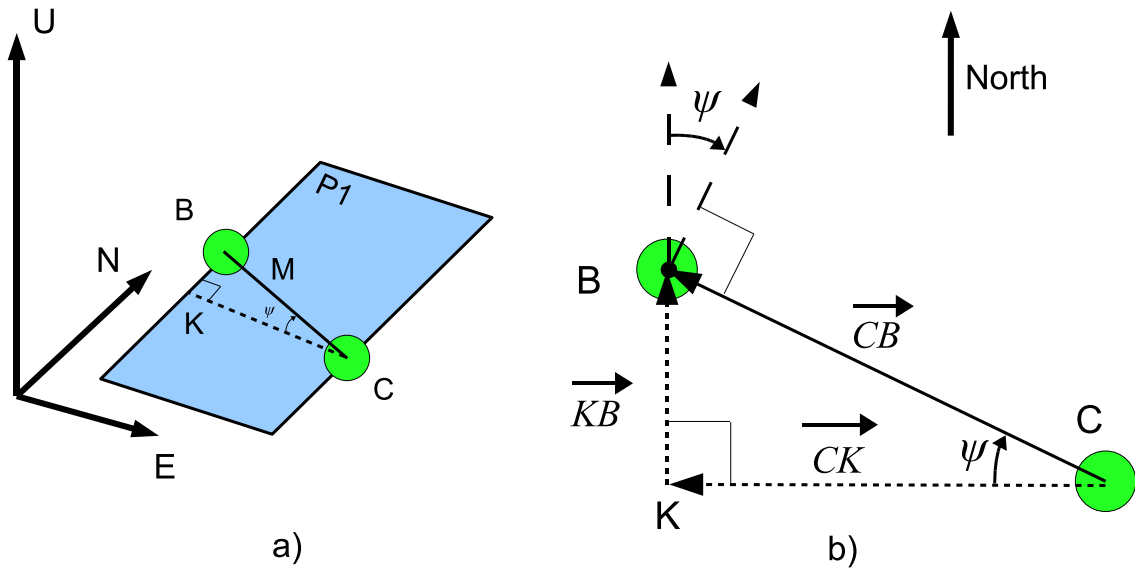


Figure 3.28: Yaw determination with two antennas available

The set of equations 3.121 is solved in an iterative process similar to positioning algorithm. Linearizing with respect to unknown variables and expressing in a matrix form with known values at the left side yields

$$omc = \begin{bmatrix} 2(e_B - e_C) & 2(n_B - n_C) \\ 2(e_B - e_A) & 2(n_B - n_A) \end{bmatrix} \cdot \begin{bmatrix} \Delta e_B \\ \Delta n_B \end{bmatrix} \quad (3.122)$$

where observed minus computed value  $omc$  is

$$omc = \begin{bmatrix} D_{BC}^2 - (u_B - u_C)^2 - (e_B - e_C)^2 - (n_B - n_C)^2 \\ D_{AB}^2 - (u_B - u_A)^2 - (e_B - e_A)^2 - (n_B - n_A)^2 \end{bmatrix} \quad (3.123)$$

The process starts from measured position B and stops when position improvements  $\Delta e_B$  and  $\Delta n_B$  are negligibly small.

For pitch determination, point M should be introduced, which is located in the middle of the vector connecting two Topcon antennas. Vector  $\overrightarrow{MA}$  connects point M with Ashtech antenna represented in the picture by letter A. The vector should be considered in plane P2 shown in Figure 3.30 a. This plane is perpendicular to the local horizontal plane. Consequently, pitch is determined as:

$$\theta = \arcsin \left( \frac{\|\overrightarrow{DA}\|}{\|\overrightarrow{MA}\|} \right) \quad (3.124)$$

To determine roll, only two antennas are needed. Two Topcon antennas are used in roll estimation. If we consider two antennas in plane P3, which is perpendicular to the local horizontal

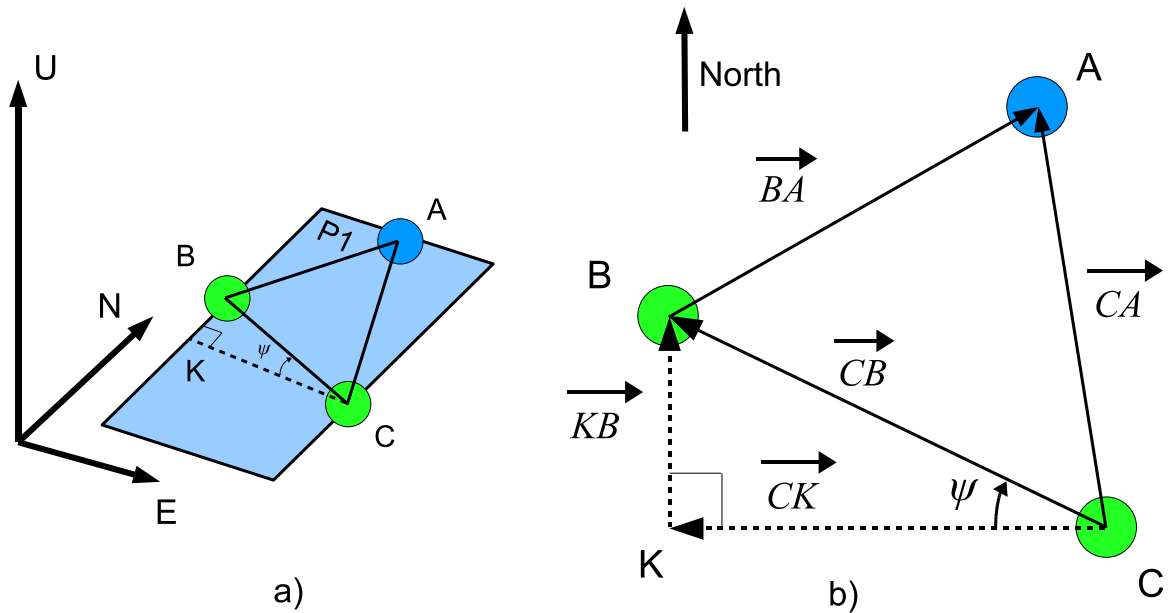


Figure 3.29: Yaw determination with three antennas available

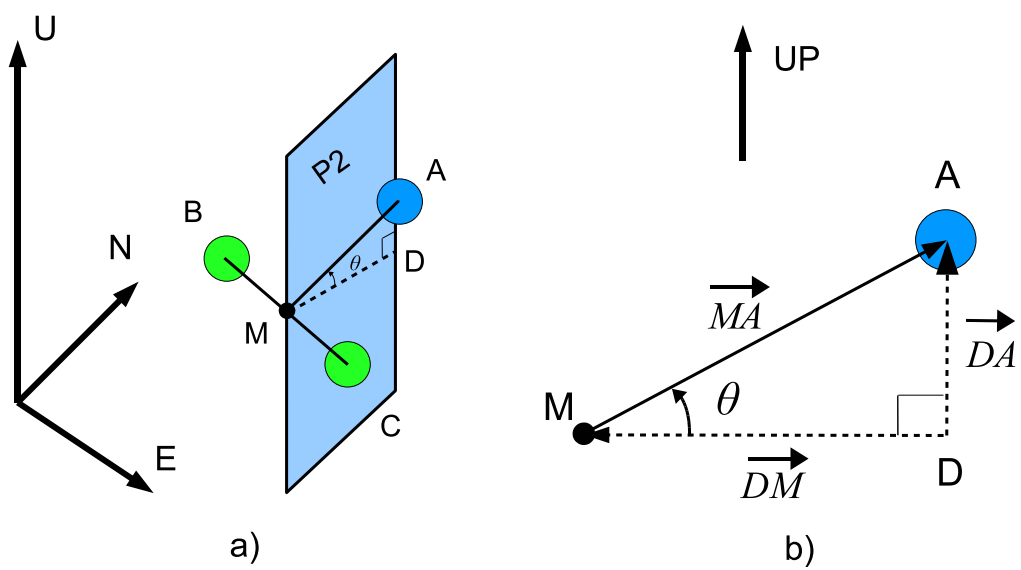


Figure 3.30: Pitch determination

## CHAPTER 3. IMPLEMENTATION

---

plane, roll can be found as (Figure 3.31):

$$\varphi = \arcsin \left( \frac{\|\overrightarrow{PB}\|}{\|\overrightarrow{CB}\|} \right) \quad (3.125)$$

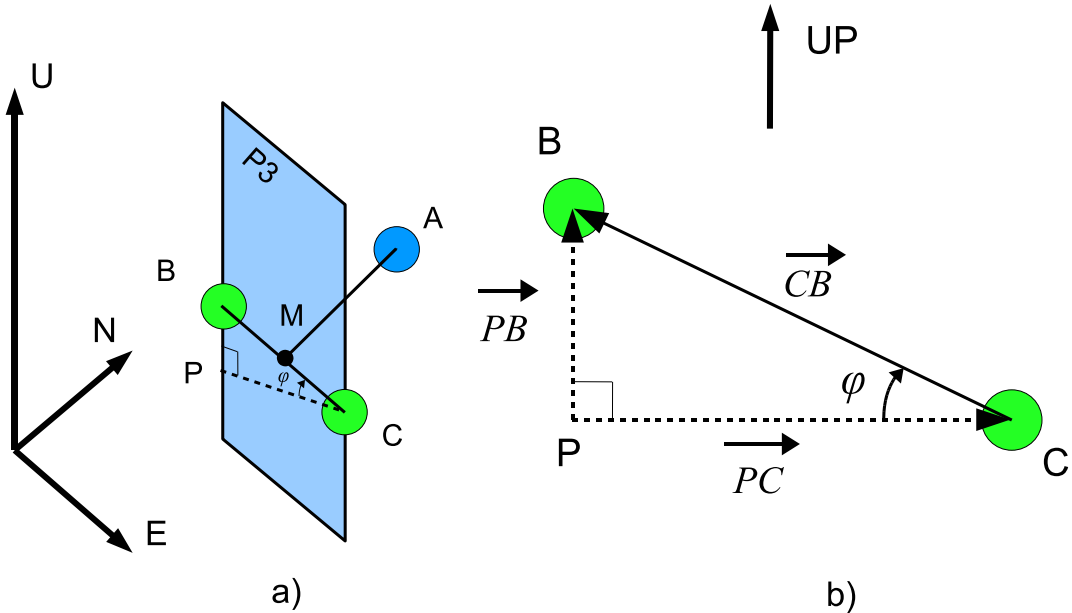


Figure 3.31: Roll determination

# Chapter 4

## Results and Discussion

The results of the conducted tests are summarized in Figures 4.1 and 4.2 for a stationary and moving master, respectively. In the subplot "UTM Coordinates" the trail of the vehicle is shown. Gray triangles in the left bottom corner show that the vehicle was stationary for some time and later it started moving toward the upper right corner. When that corner was reached, the vehicle turned left and continued moving toward the left bottom corner. The test was conducted on the field and the vehicle was moving along the roads made for spraying. Ideally, those roads have to be parallel with 20 meters separation. Subplots "Roll", "Pitch", and "Yaw" represent the change of the respective angles over time. The variation in all three angles is relatively small during the first 60 seconds which corresponds to the stationary position of the vehicle.

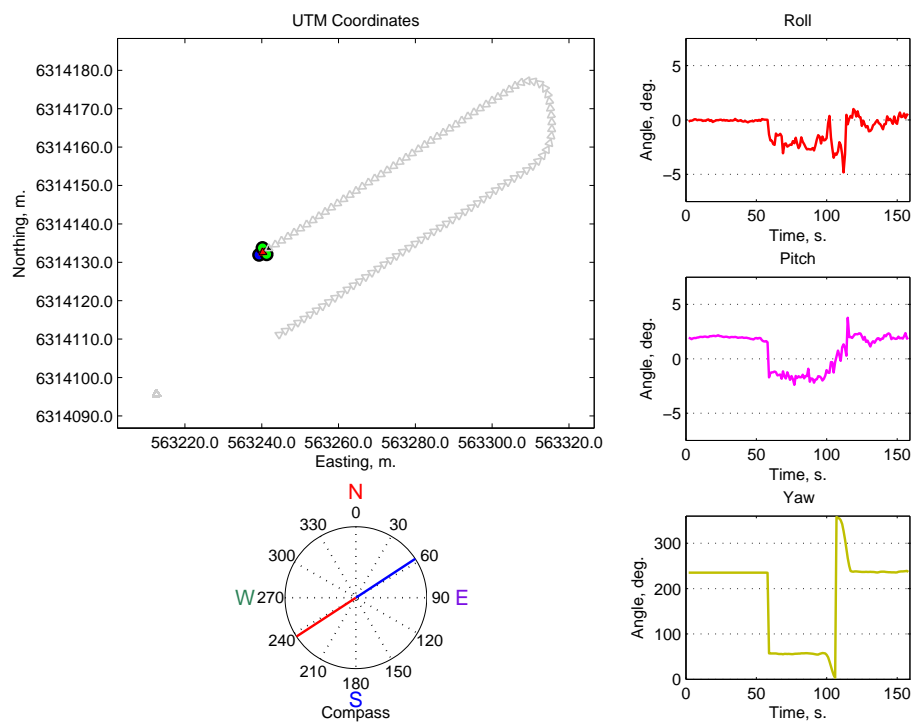


Figure 4.1: Attitude determination with three antennas available. Differential positions are computed by a Kalman filer with stationary master

After being stationary for 60 seconds, the vehicle started moving. Roll values close to  $-2^\circ$  show that the right side of the vehicle was a little higher than the left side, while the variation of approximately  $\pm 1^\circ$  corresponds to the irregularity of the ground road. Around the time of 120 seconds the vehicle changed direction of movement. After the turn the roll values remain close to  $0^\circ$  due to the topography.

## CHAPTER 4. RESULTS AND DISCUSSION

---

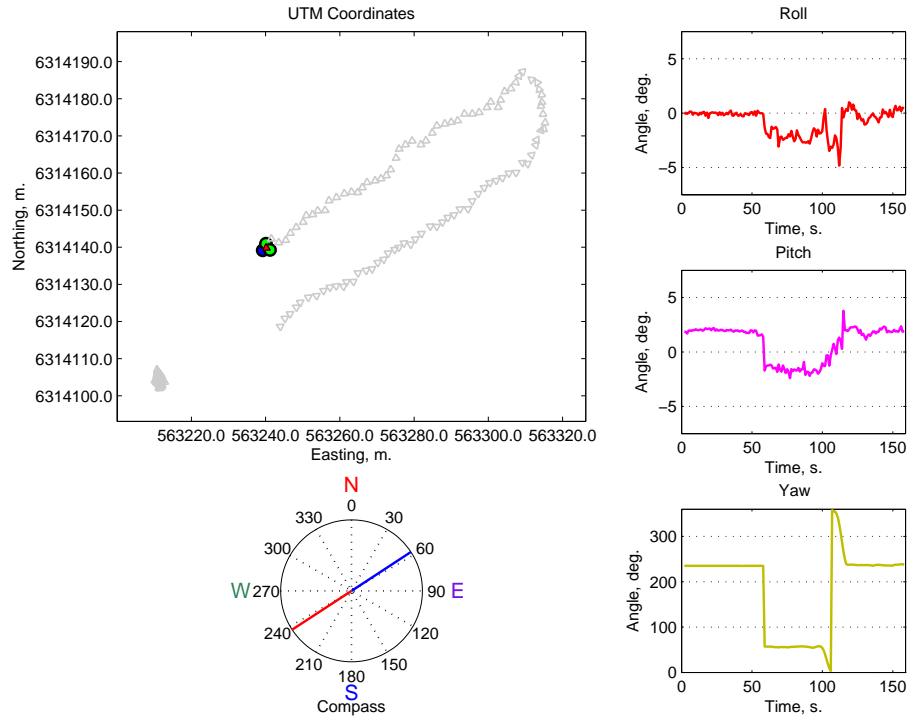


Figure 4.2: Attitude determination with three antennas available. Positions are computed by a Kalman filer using one of the antennas on the tractor as a master

Pitch values close to  $2^\circ$  during the first 60 s correspond to the position of the vehicle with the front side being higher. During the next 60 s the vehicle was moving downhill while after the turn it was moving uphill again.

During the time when the vehicle was stationary the heading was close to  $235^\circ$  North. In the time period from 60 s till 100 s the vehicle was moving with yaw close to  $60^\circ$ . The turn lasted for almost 20 s, and the vertical line from  $0^\circ$  to  $360^\circ$  means that the vehicle crossed the northern direction. From 120 s till the end of the observation the heading of the vehicle remained almost constant. The yaw separation of  $180^\circ$  before and after the turn means that the vehicle was moving along the parallel lines.

The last subplot is called Compass. The subplot represents the heading of the vehicle. The idea behind this subplot is to show the heading of the vehicle as it would be shown by an ordinary compass located inside the vehicle in real time.

Figure 4.3 represents roll, pitch, and yaw angles obtained by the Kalman filter and least-squares solution at the top of the figure and at the bottom, respectively. Accuracies of the angles are shown in Table 4.1. Standard deviation  $\sigma$  is computed according to the following formula

$$\sigma = \sqrt{\frac{1}{n-1} \sum_{i=1}^n (x_i - \bar{x})^2} \quad (4.1)$$

where

$$\bar{x} = \frac{1}{n} \sum_{i=1}^n x_i \quad (4.2)$$

This is not a true standard deviation of the results obtained by a Kalman filter. However, it can be proven mathematically that this standard deviation is larger than the true one.

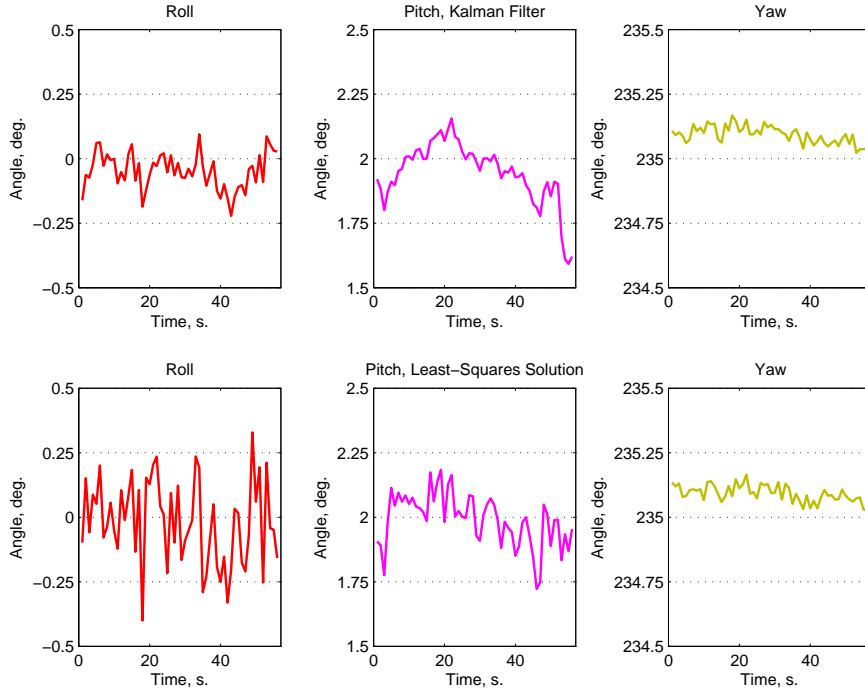


Figure 4.3: Attitude determination, stationary master

Table 4.1: Attitude accuracy,  $2\sigma$ -level, 2 m antenna separation, stationary master, deg

Method \ Angles	Roll	Pitch	Yaw
Kalman filter	0.140	0.241	0.066
least-squares solution	0.327	0.204	0.064

Figure 4.4 shows yaw angles calculated by the Kalman filter and least-squares solution when two and three antennas were used in the angle calculation. The best result is obtained when the heading is calculated from the positions of all three antennas determined by the Kalman filter, while the worst result is when the yaw is calculated only from positions of two antennas determined by least-squares solution. Table 4.2 summarizes  $2\sigma$  level accuracies of the angles shown in Figure 4.4.

Figure 4.5 represents attitude angles obtained by the Kalman filter and least-squares solution with the moving master receiver. In this case one of the antennas mounted on the vehicle is used

## CHAPTER 4. RESULTS AND DISCUSSION

---

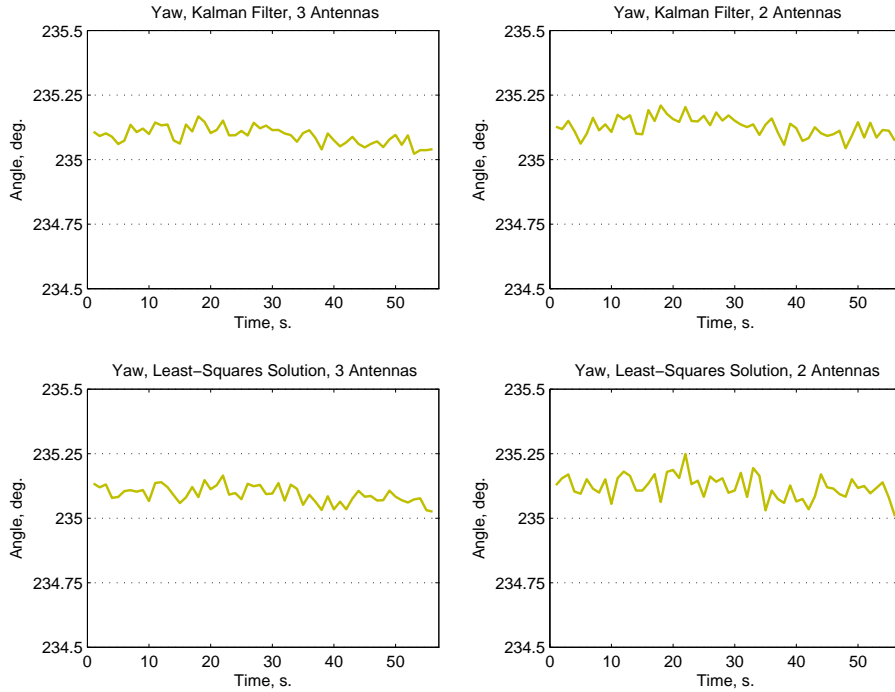


Figure 4.4: Heading accuracy with two and three antennas available, stationary master

Table 4.2: Yaw accuracy,  $2\sigma$ -level, 2 m antenna separation, stationary master, deg

Method \ Antennas used	Three antennas	Two antennas
Kalman filter	0.066	0.073
least-squares solution	0.064	0.092

as a master. Accuracies of the angles are shown in Table 4.3. It can be seen in the table that the accuracy of the angles obtained from the Kalman filter is lower with moving master compared to the accuracies of the angles with the stationary master. However, the accuracy of the angles calculated from the positions obtained with least-squares solution remains the same.

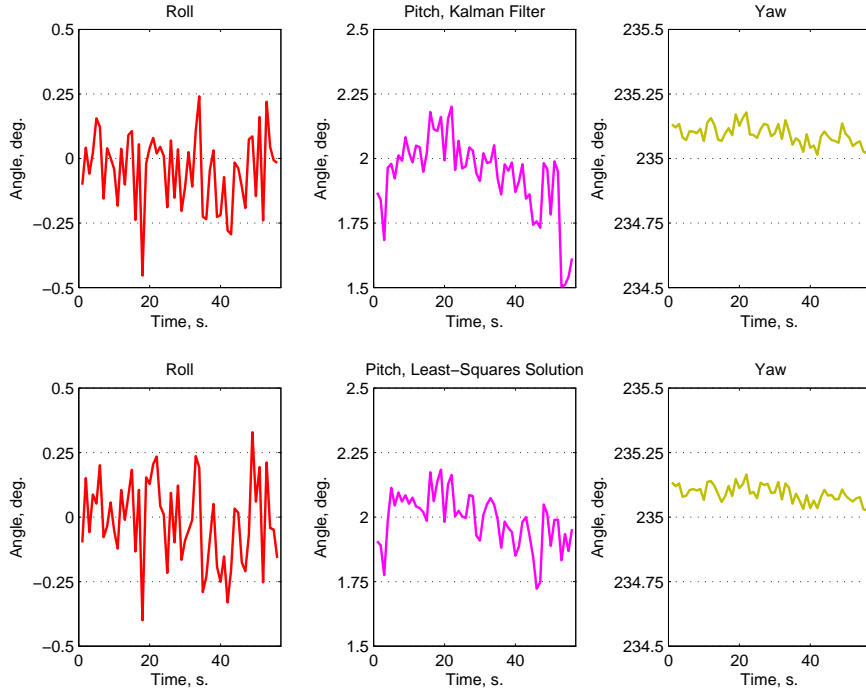


Figure 4.5: Attitude determination, moving master

Table 4.3: Attitude accuracy,  $2\sigma$ -level, 2 m antenna separation, moving master, deg

Method \ Angles	Roll	Pitch	Yaw
Kalman filter	0.283	0.308	0.075
least-squares solution	0.327	0.204	0.064

Figure 4.6 shows yaw angles calculated by the Kalman filter and least-squares solution from positions of two or three antennas with moving master. In this case the best result is obtained when the heading is calculated from the positions of all three antennas determined by least-squares solution while the worst result is when the yaw is calculated only from positions of two antennas determined by the Kalman filter. Table 4.4 summarizes  $2\sigma$ -level accuracies of the angles shown in Figure 4.6.

Figures 4.7, 4.8, 4.9, 4.10 present precisions and coordinate deviations from the mean of positions computed by the Kalman filter and least-squares solution when master is a stationary receiver. Table 4.5 summarizes position precisions.

## CHAPTER 4. RESULTS AND DISCUSSION

---

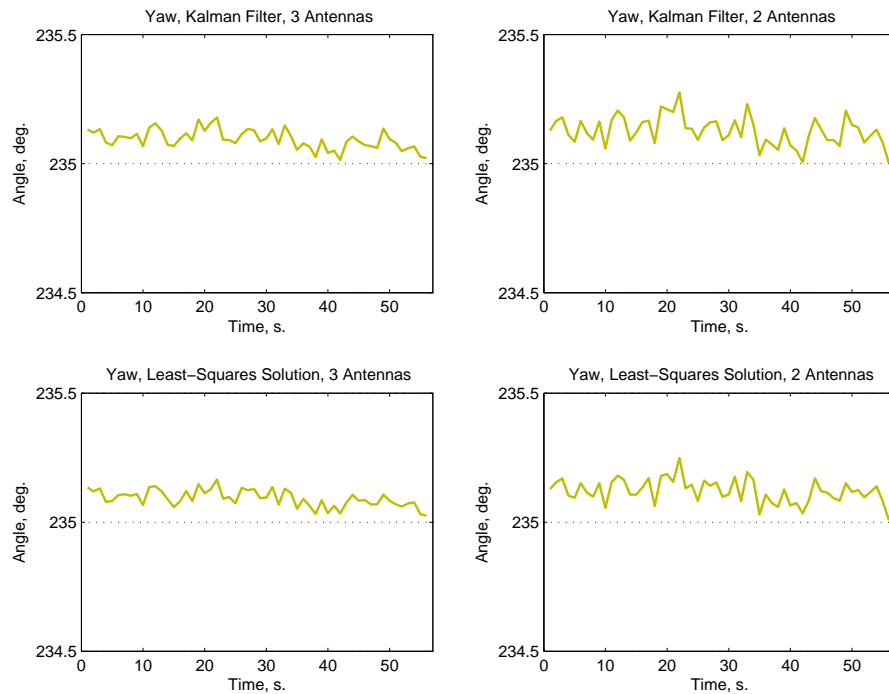


Figure 4.6: Heading accuracy with two and three antennas available, moving master

Table 4.4: Yaw accuracy,  $2\sigma$ -level, 2 m antenna separation, moving master, deg

Method \ Antennas used	Three antennas	Two antennas
Kalman filter	0.075	0.112
least-squares solution	0.064	0.092

Table 4.5: Position accuracy,  $2\sigma$ -level, m

Method	Accuracy
Kalman filter	0.009
least-squares solution	0.017

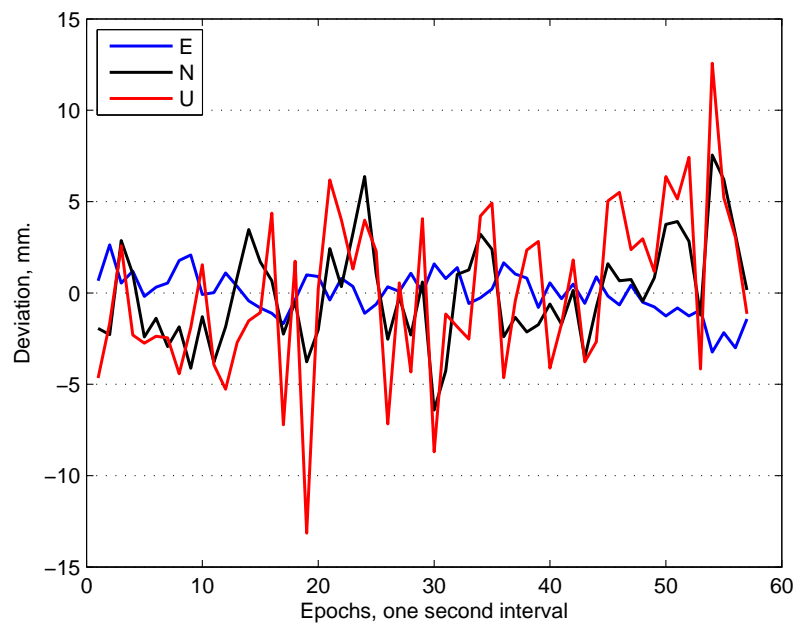


Figure 4.7: Deviation from the mean position, least-squares solution

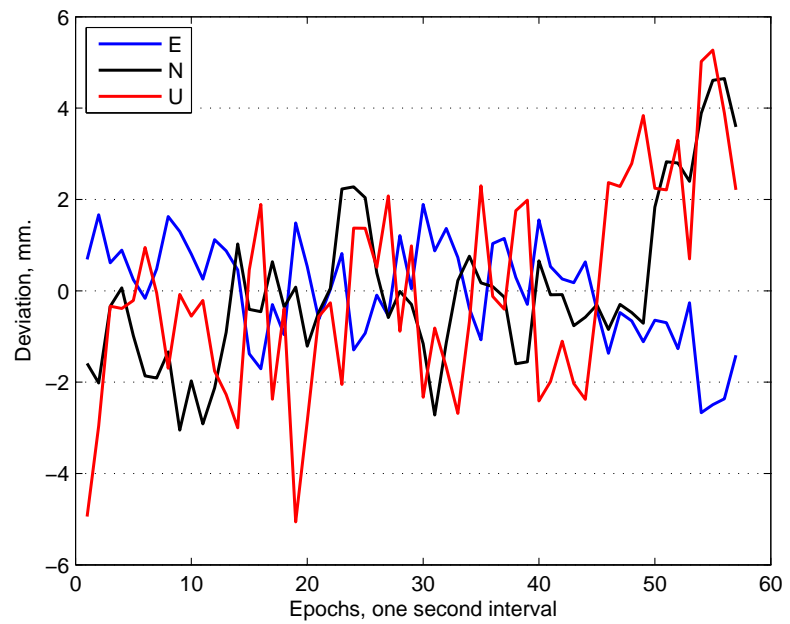


Figure 4.8: Deviation from the mean position, Kalman filter

## CHAPTER 4. RESULTS AND DISCUSSION

---

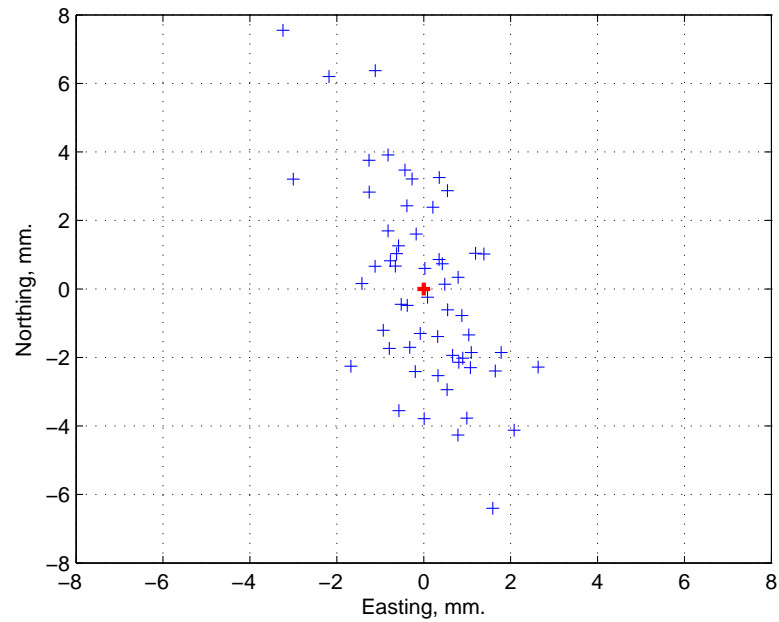


Figure 4.9: Least-squares solution, stationary master

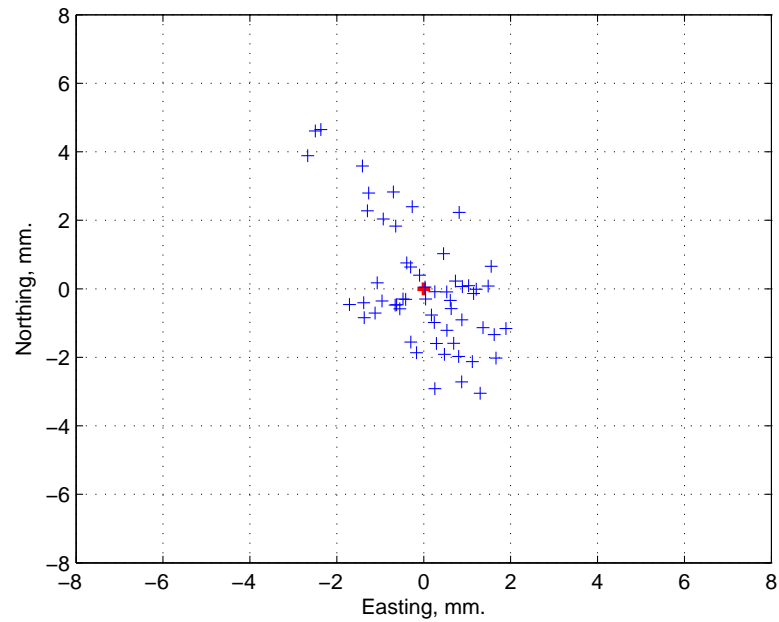


Figure 4.10: Kalman filter, stationary master

---

Figures 4.11 and 4.12 illustrate precisions of positions which are used in attitude determination when one of the antennas on the tractor is taken as a master. The precision is low, nevertheless, the attitude is determined accurately. Attitude determination is based on directions of the baselines connecting the antennas on the vehicle. The error in the master position does not affect the baseline estimation. Therefore, computing one of the antennas' position in a stand alone-mode and assuming it as a master station still make it possible to determine attitudes accurately. Figures 4.13 and 4.14 present coordinate variations of the baselines connecting two antennas of the stationary tractor.

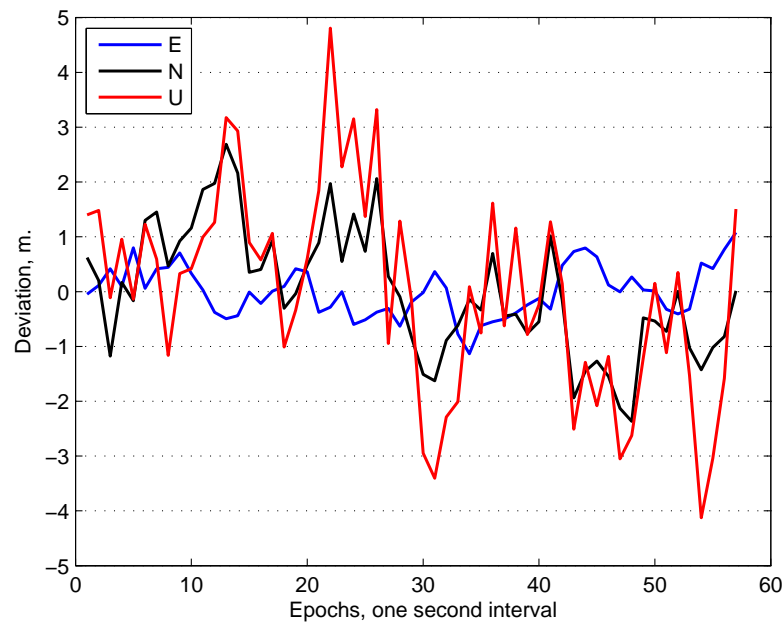


Figure 4.11: Deviation from the mean position, least-squares solution

Our 9<sup>th</sup> semester project was used to find true position of the stationary master applying EGNOS corrections. The results of position computation are depicted in Figures 4.15 and 4.16. The accuracy is in the range of two meters after the Kalman filter converged.

## CHAPTER 4. RESULTS AND DISCUSSION

---

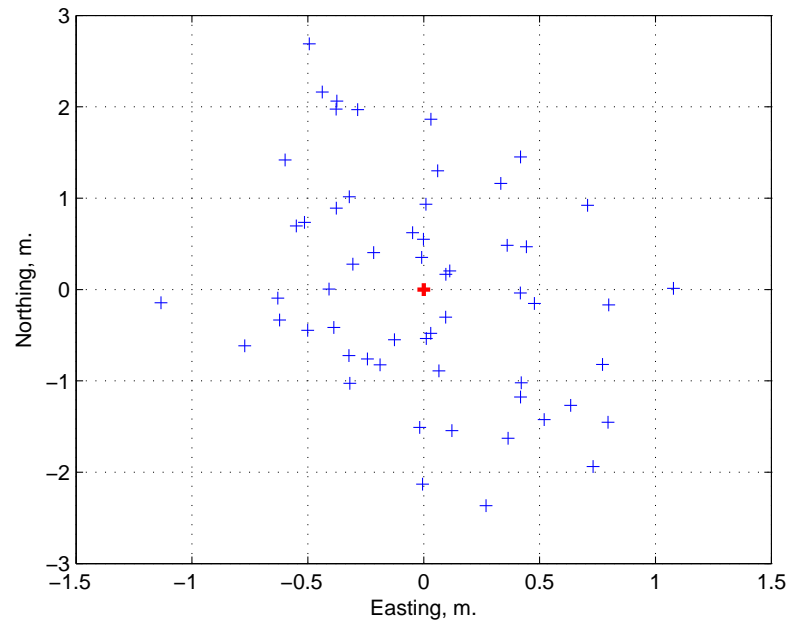


Figure 4.12: Least-squares solution

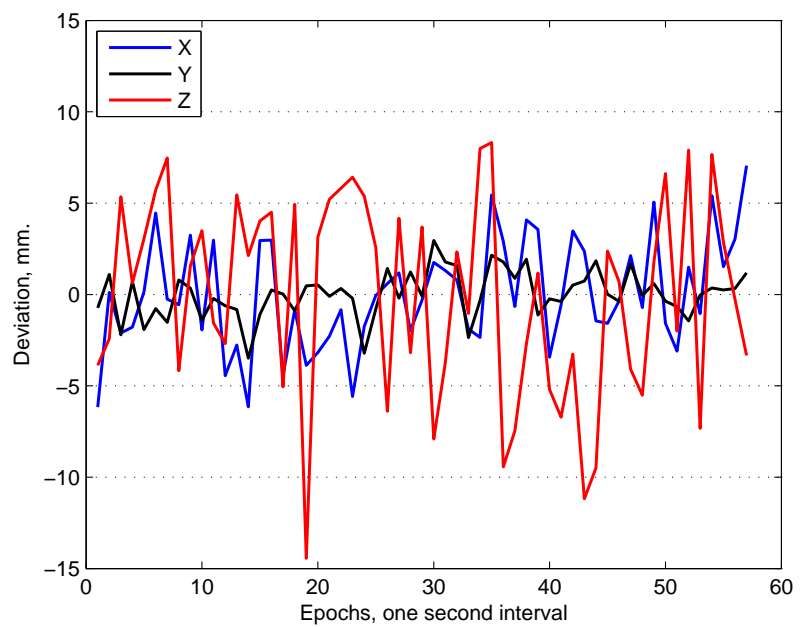


Figure 4.13: Deviation of the distance between antennas 1 and 2 from the mean,  
Kalman filter

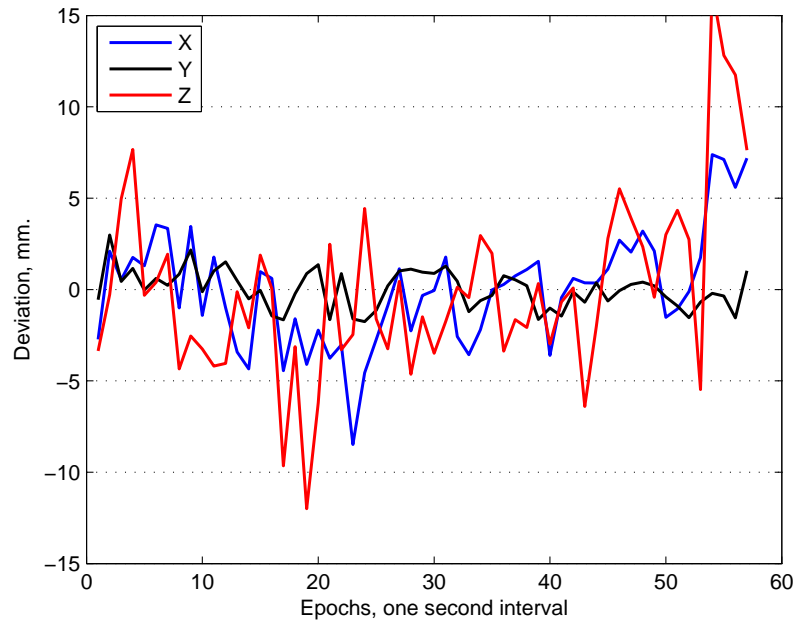


Figure 4.14: Deviation of the distance between antennas 1 and 3 from the mean, Kalman filter

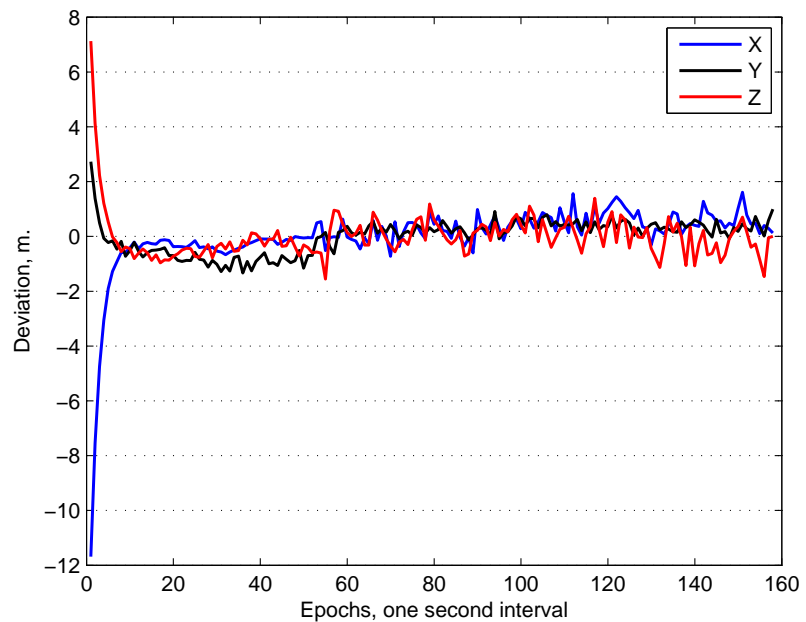


Figure 4.15: Deviation from the mean position, master receiver

## CHAPTER 4. RESULTS AND DISCUSSION

---

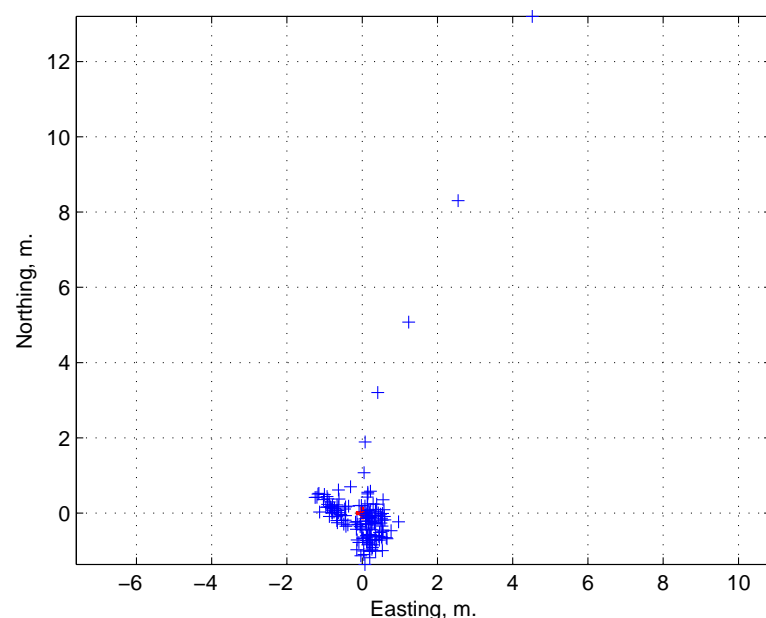


Figure 4.16: Master receiver position

# Chapter 5

## Conclusions

Carrier phase observations were implemented in a software receiver running in post processing mode. The carrier phase observations are quite noisy, therefore, the positions have high errors in the range of a few thousand meters. High accuracy of positioning could be achieved by implementing a specific PLL loop for precise carrier phase tracking.

The GPS positioning methods and cases of operation we have investigated can be divided into the following groups:

- Master station position estimation using EGNOS corrections
- Ambiguity resolution of carrier phase observations
- Cycle slip detection
- Implementation of a Kalman filter for positioning
- Heading determination using two receivers on a vehicle
- Attitude determination using three receivers on a vehicle
- Precise positioning and heading determination using master station and two receivers on a vehicle
- Precise positioning and attitude determination using master station and three receivers on a vehicle.

Based on the data presented in this section we can make a conclusion that positions calculated with stationary master are much more accurate than with the moving master. However, for attitude determination only relative location of antennas mounted on a vehicle is important but not the true position of the antennas. Therefore, accuracies of the attitude angles calculated with stationary and moving master are similar.

In conclusion, we have achieved our goals defined in the project problem description. The positioning methods explored were deployed in a static and kinematic mode. An ambiguity resolution was successfully examined with good results in differential positioning. This project follows a consistent way of building up a working satellite based positioning system.

### 5.1 Future Considerations and Improvements

In future the project could be improved by implementation of items listed below:

## CHAPTER 5. CONCLUSIONS

---

- Real-time implementation of the developed software.
- Determination of cycle slips to repair the ambiguity resolution of carrier phase observations
- Improvement of the ambiguity resolution method by including the geometry of the antennas
- Implementation of a Kalman filter for positioning which includes the geometry of the antennas
- Code porting from Matlab to C or other language providing fast runtime execution. This may benefit in making the software stand alone, as it now requires Matlab in order to execute. Additionally embedded systems are neither able to support Matlab nor have the computational power to run interpreted code
- Development of a more precise PLL tracking loop in the software receiver which will provide more precise carrier phase observations compared to code phase observations.

# Appendix A

## Data contained in the DVD

The included DVD contains all GUIs, functions, and observation data presented in the report. File `track6sats.ra4` contains raw GPS observations downloaded from the receivers. The recorded by the front end signal is stored in a file `3dvd.bin`. This file has only a part of the whole recorded signal because it's size is 5.4 GB: this is above the DVD+R disc size. SiSNet logged messages are saved in file `h16_cut.ems`.

All functions have short descriptions at the beginning of their codes. They are called by GUIs whenever necessary.

The main functions used in the project are listed as follows

- `postProcessing.m` – acquisition and tracking of EGNOS satellites
- `carrpprat.m` – positioning based on software receiver carrier phase observations generated from PLL output frequencies
- `carphase.m` – positioning based on software receiver carrier phase observations simulated from ephemerides
- `S10FuIonEgKalm.m` – master position estimation using EGNOS corrections
- `S10KalmI_SB3Rs.m` – positioning and attitude determination using stationary master
- `S10KalmI_MB3Rs.m` – attitude determination using moving master.

# **Appendix B**

## **Working Process**

After analyzing the whole task of the project, the work was divided into the following main parts: carrier observations in a software receiver, master station position estimation using EGNOS corrections, precise positioning and attitude determination. SiSNet service was used to lodge EGNOS messages, and our 9<sup>th</sup> semester project was used to apply the corrections.

There are only two members in our group, so we did not actually create any timetable due to constantly changing expectations and tasks of the project, especially concerning the part of the project related to a software receiver. At the beginning of the project we wanted to implement carrier phase observations in a software receiver to provide precise positioning. But it turned out to be rather difficult task. Therefore, we decided to process carrier phase observations made by professional geodetic receivers. Eventually, we succeeded in the implementation of carrier phase observations in a software receiver, however, the results are not satisfactory. The implementation with results were included to present the nature of carrier phase observations. Group meetings with our supervisor were organized not systematically but whenever necessary.

In conclusion, small groups are not capable of doing large projects, however, the efficiency per member is higher in small groups due to much easier coordination.

# Bibliography

- [B. 01] B. Hoffmann-Wellenhof, H. Lichtenegger, & J. Collins. *GPS Theory and Practice*. Springer-Verlag Wien New York, 2001.
- [Bor97] Gilbert Strang & Kai Borre. *Linear Algebra, Geodesy, and GPS*. Wellesley-Cambridge Press, 1997.
- [Eng01] Pratap Misra & Per Enge. *Global Positioning System. Signals, Measurements, and Performance*. Ganga-Jamuna Press, 2001.
- [Jam96] James J. Spilker Jr. & Bradford W. Parkinson, editor. *Global Positioning System: Theory and Application*, volume 2. American Institute of Aeronautics, Inc., 1996.
- [Kai07] Kai Borre, Dennis Akos, Nicolaj Bertelsen, Peter Rinder, & Søren Holdt Jensen. *A Software-Defined GPS and Galileo Receiver. Single-Frequency Approach*. Birkhäuser, 2007.
- [Kap96] Elliott D. Kaplan. *Understanding GPS: Principles and Applications*. Artech House, Inc., 1996.
- [Lei04] Alfred Leick. *GPS Satellite Surveying*. John Wiley & Sons, Inc., third edition, 2004.
- [McC06] Dennis D. McCarthy. Iers conventions (1996). IERS Technical Note 21, International Earth Rotation and Reference Systems Service, Available at: <http://maia.usno.navy.mil/conventions.html>, July 1996 (accessed April 3, 2006).
- [Nat06] National Geospatial-Intelligence Agency. Implementation of the World Geodetic System 1984 (WGS 84) Reference Frame G1150. Addendum to NIMA TR 8350.2, Available at: <http://earth-info.nga.mil/GandG/publications/tr8350.2/Addendum%20NIMA%20TR8350.2.pdf>, 23 June 2004 (accessed April 29, 2006).
- [Ser06] ARINC Engineering Services. Navstar GPS Space Segment/Navigation User Interfaces. Interface specification IS-GPS-200, Rev. D (Public Release Version), Available at: <http://www.navcen.uscg.gov/gps/geninfo/IS-GPS-200D.pdf>, 7 December 2004 (accessed May 6, 2006).
- [Sic01] John Van Sickle. *GPS for Land Surveyors*. Taylor & Francis Group., second edition, 2001.

# List of Tables

1.1	Overall error budget . . . . .	7
1.2	Components of satellite signal . . . . .	8
3.1	Ephemeris parameters and definitions . . . . .	17
3.2	DOP factors and their implications . . . . .	37
4.1	Attitude accuracy, $2\sigma$ -level, 2 m antenna separation, stationary master, deg . . . . .	55
4.2	Yaw accuracy, $2\sigma$ -level, 2 m antenna separation, stationary master, deg . . . . .	56
4.3	Attitude accuracy, $2\sigma$ -level, 2 m antenna separation, moving master, deg . . . . .	57
4.4	Yaw accuracy, $2\sigma$ -level, 2 m antenna separation, moving master, deg . . . . .	58
4.5	Position accuracy, $2\sigma$ -level, m . . . . .	58

# List of Figures

3.1	The WGS 84 Coordinate System Definition . . . . .	11
3.2	Elements of the Keplerian orbits ( $a, e, i, l, \omega, v$ ) . . . . .	14
3.3	Elliptic Keplerian orbit . . . . .	15
3.4	C/A-code generation . . . . .	20
3.5	Autocorrelation of C/A-code with PRN 2 . . . . .	21
3.6	Cross-correlation of C/A-codes with PRN 2 and 12 . . . . .	21
3.7	Block diagram of parallel code phase search algorithm [Kai07] . . . . .	22
3.8	Acquisition of EGNOS satellite with PRN 26 . . . . .	23
3.9	Acquisition of all satellites . . . . .	24
3.10	Block diagram of parallel frequency space search algorithm [Kai07] . . . . .	24
3.11	Fine carrier frequency estimation . . . . .	25
3.12	Tracking channel [Kai07] . . . . .	26
3.13	Tracking results of satellite PRN 5 . . . . .	27
3.14	PLL and DLL discriminators of tracking satellite PRN 5 . . . . .	27
3.15	Pseudorange measurement . . . . .	28
3.16	Pseudoranges . . . . .	29
3.17	Generated carrier based on PLL output frequency . . . . .	32
3.18	Positioning based on code phase and carrier phase observations . . . . .	33
3.19	Carrier phase observations based on PLL output frequencies . . . . .	33
3.20	Carrier phase observations based on frequencies from satellite velocities . . . . .	34
3.21	Positioning based on code phase and carrier phase observations . . . . .	35
3.22	Differential positioning . . . . .	38
3.23	Rate of difference between carrier phase observations on L1 and L2 without cycle slips . . . . .	44
3.24	Rate of difference between carrier phase observations on L1 and L2 with cycle slips . . . . .	45
3.25	Attitude geometry. Courtesy of [Jam96] . . . . .	47
3.26	Coordinate frames and rotation eagles . . . . .	48
3.27	Location of GPS antennas on a vehicle . . . . .	49
3.28	Yaw determination with two antennas available . . . . .	50
3.29	Yaw determination with three antennas available . . . . .	51
3.30	Pitch determination . . . . .	51
3.31	Roll determination . . . . .	52
4.1	Attitude determination with three antennas available. Differential positions are computed by a Kalman filer with stationary master . . . . .	53

## LIST OF FIGURES

---

4.2	Attitude determination with three antennas available. Positions are computed by a Kalman filer using one of the antennas on the tractor as a master . . . . .	54
4.3	Attitude determination, stationary master . . . . .	55
4.4	Heading accuracy with two and three antennas available, stationary master . . . . .	56
4.5	Attitude determination, moving master . . . . .	57
4.6	Heading accuracy with two and three antennas available, moving master . . . . .	58
4.7	Deviation from the mean position, least-squares solution . . . . .	59
4.8	Deviation from the mean position, Kalman filter . . . . .	59
4.9	Least-squares solution, stationary master . . . . .	60
4.10	Kalman filter, stationary master . . . . .	60
4.11	Deviation from the mean position, least-squares solution . . . . .	61
4.12	Least-squares solution . . . . .	62
4.13	Deviation of the distance between antennas 1 and 2 from the mean, Kalman filter	62
4.14	Deviation of the distance between antennas 1 and 3 from the mean, Kalman filter	63
4.15	Deviation from the mean position, master receiver . . . . .	63
4.16	Master receiver position . . . . .	64